Electronic Supplementary Material (ESI) for Inorganic Chemistry Frontiers.

When Ferrocene and Diiron Organometallics Meet: Triiron Vinyliminium Complexes Exhibit Strong Cytotoxicity and Cancer Cell Selectivity

Silvia Schoch, Simona Braccini, Lorenzo Biancalana, Alessandro Pratesi, Tiziana Funaioli, Stefano Zacchini, Guido Pampaloni, Federica Chiellini and Fabio Marchetti

Supporting Information

Table of contents *Pages*

Figure S1. IR spectrum of **[2a]CF_3SO_3** in CH_2Cl_2 solution.

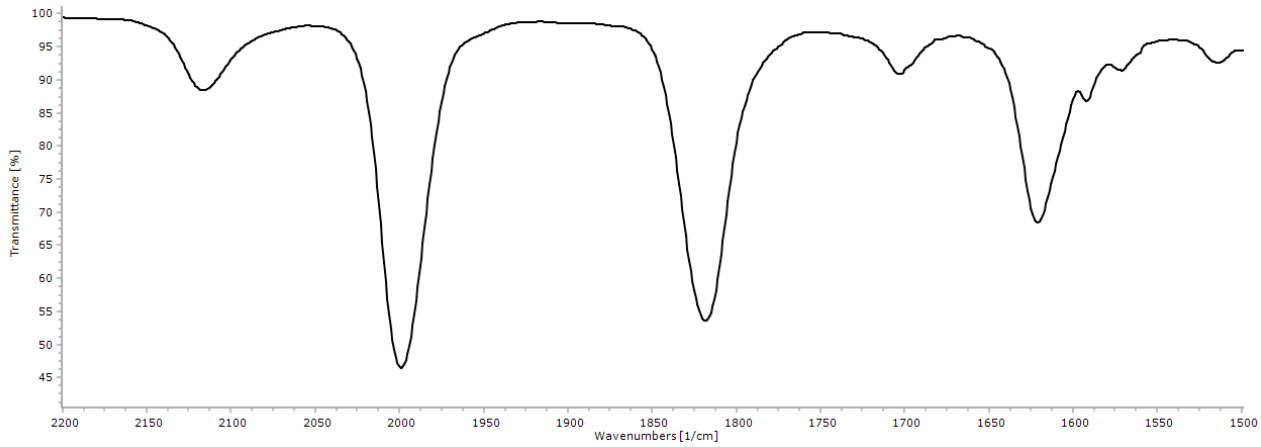

Figure S2. IR spectrum of **[2b]CF_3SO_3** in CH_2Cl_2 solution.

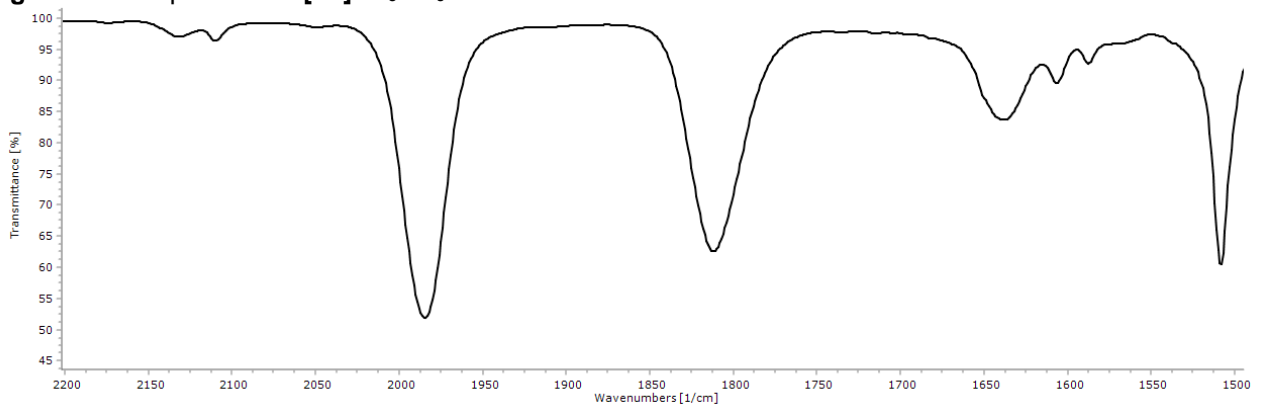

Figure S3. IR spectrum of **[2c]CF_3SO_3** in CH_2Cl_2 solution.

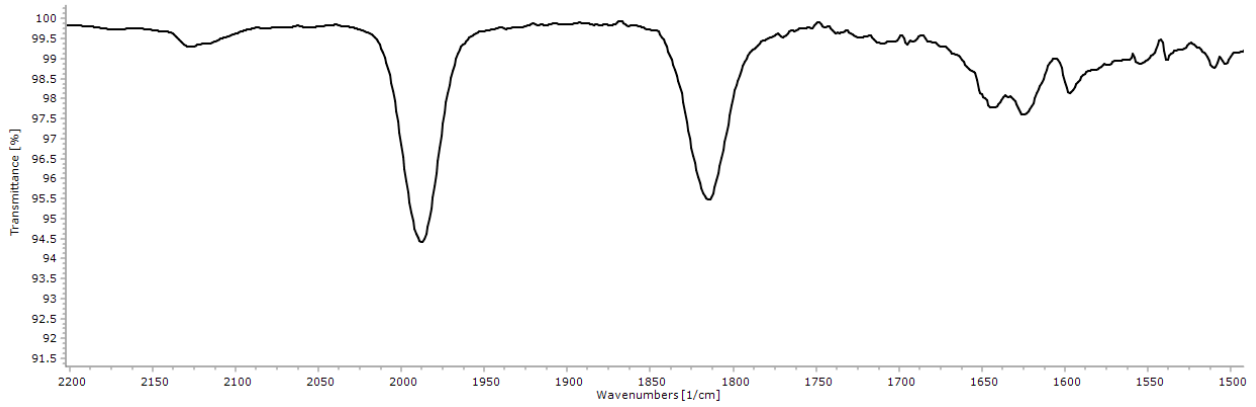

Figure S4. IR spectrum of **[2d]CF_3SO_3** in CH_2Cl_2 solution.

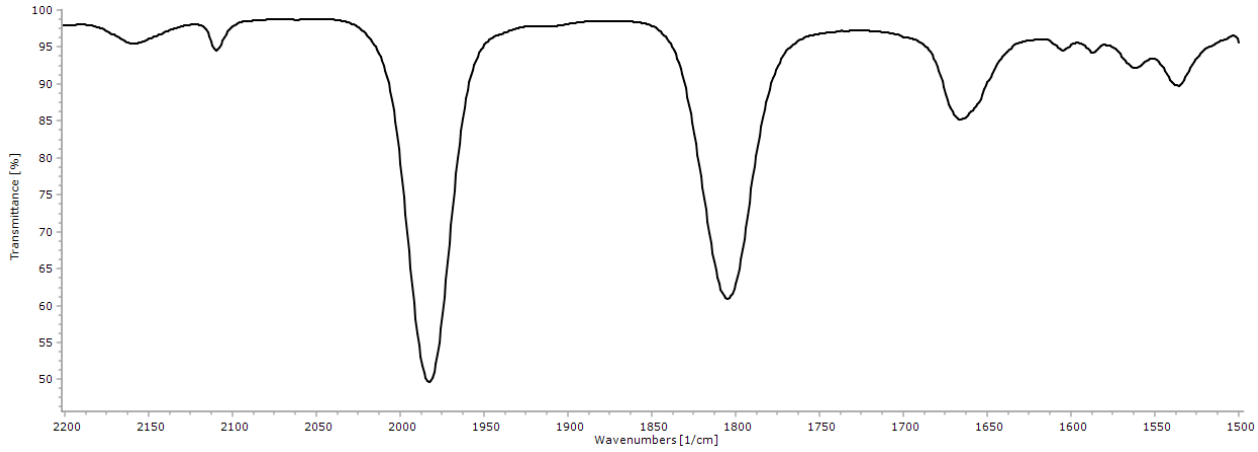

Figure S5. IR spectrum of **[2e]CF_3SO_3** in CH_2Cl_2 solution.

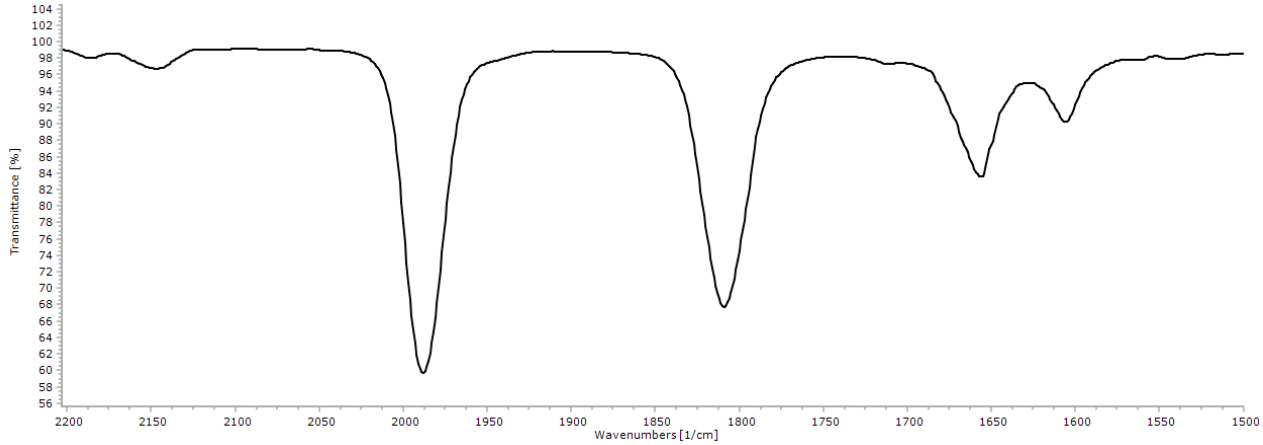

Figure S6. IR spectrum of **[2f]CF_3SO_3** in CH_2Cl_2 solution.

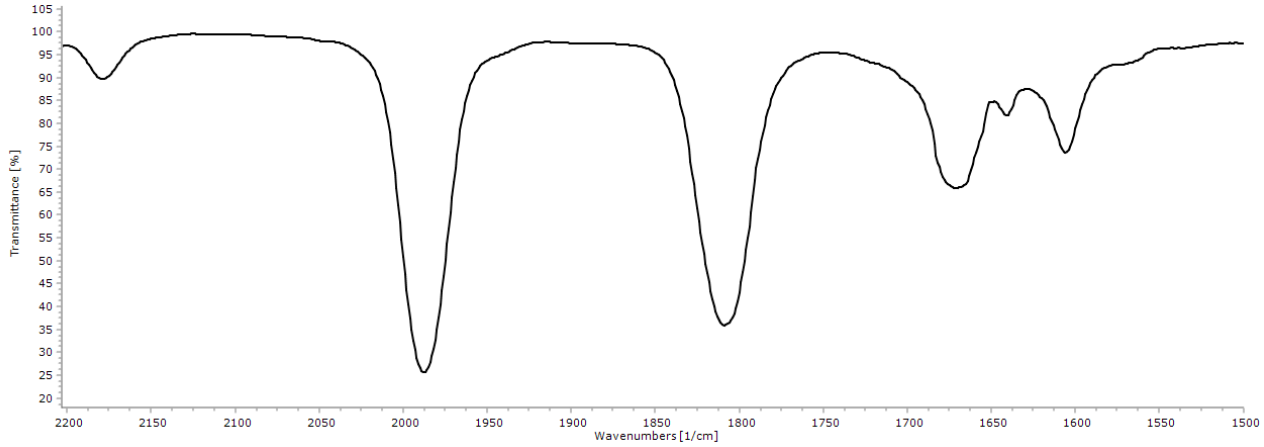

Figure S7. IR spectrum of **[2g]CF_3SO_3** in CH_2Cl_2 solution.

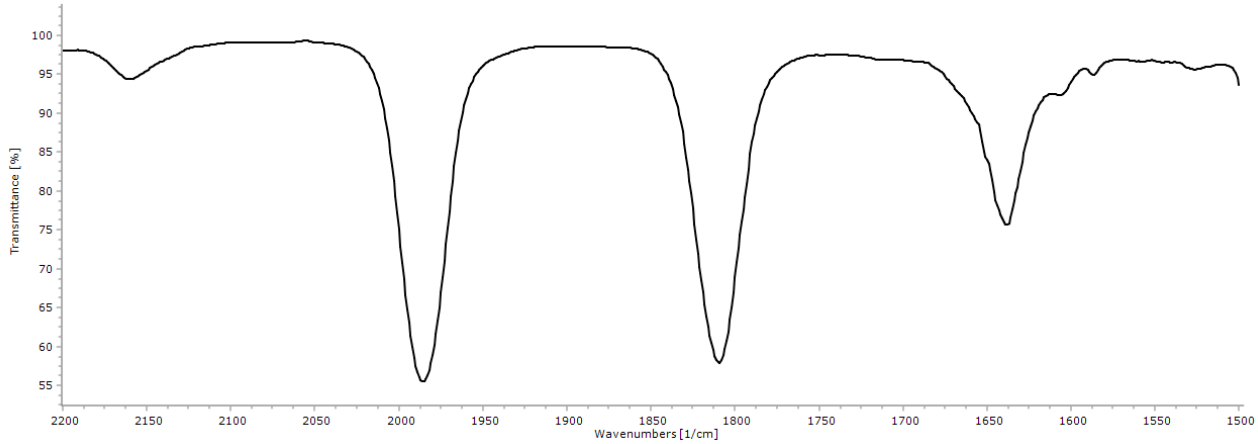

Figure S8. IR spectrum of **[2h]CF_3SO_3** in CH_2Cl_2 solution.

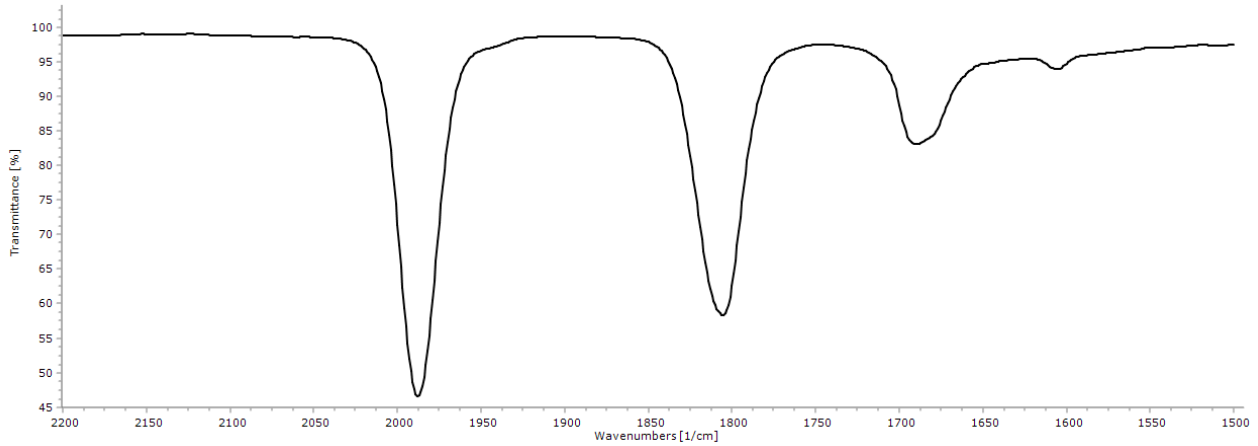

Figure S9. IR spectrum of **[2h]CF_3SO_3** in the solid state.

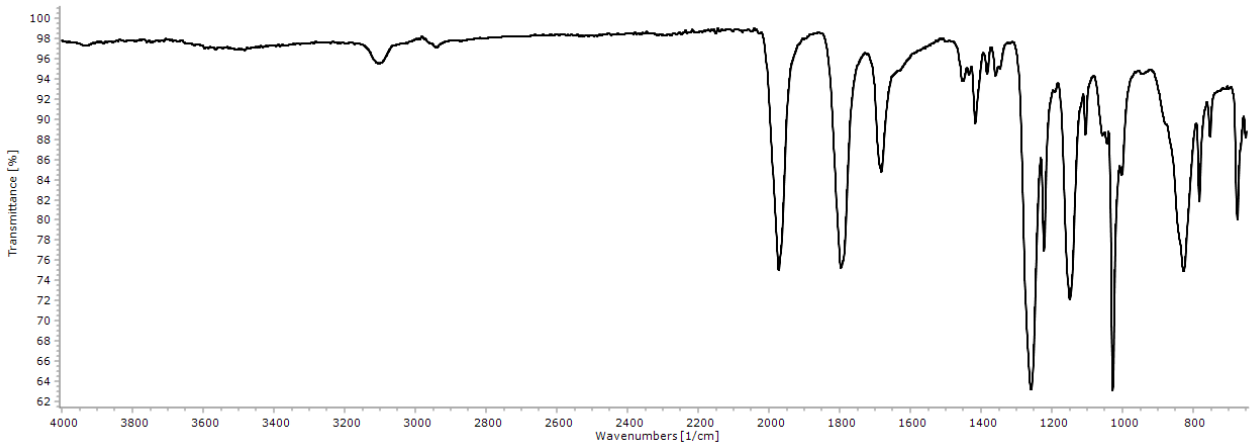

Figure S10. IR spectrum of **[2i]CF_3SO_3** in CH_2Cl_2 solution.

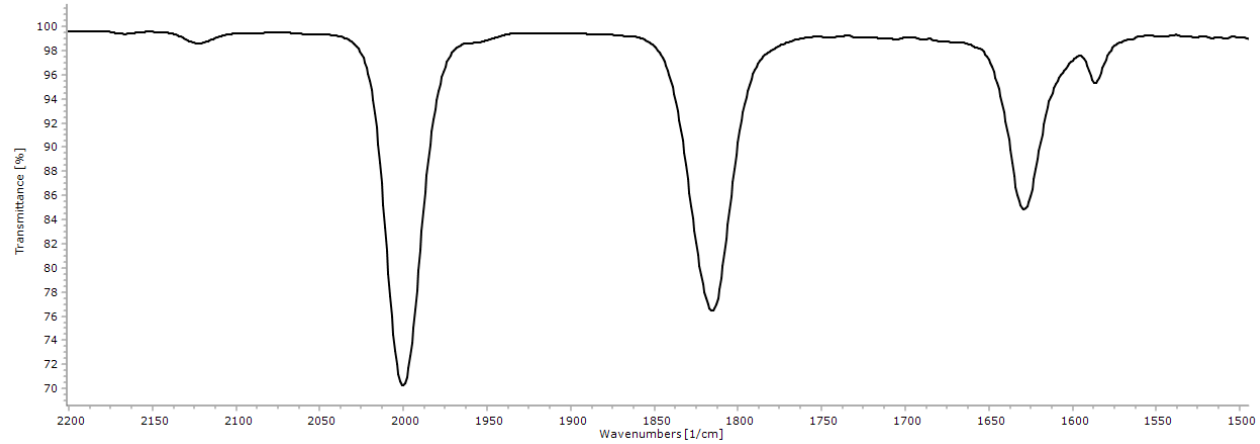

Figure S11. IR spectrum of **[2h]NO_3** in CH_2Cl_2 solution.

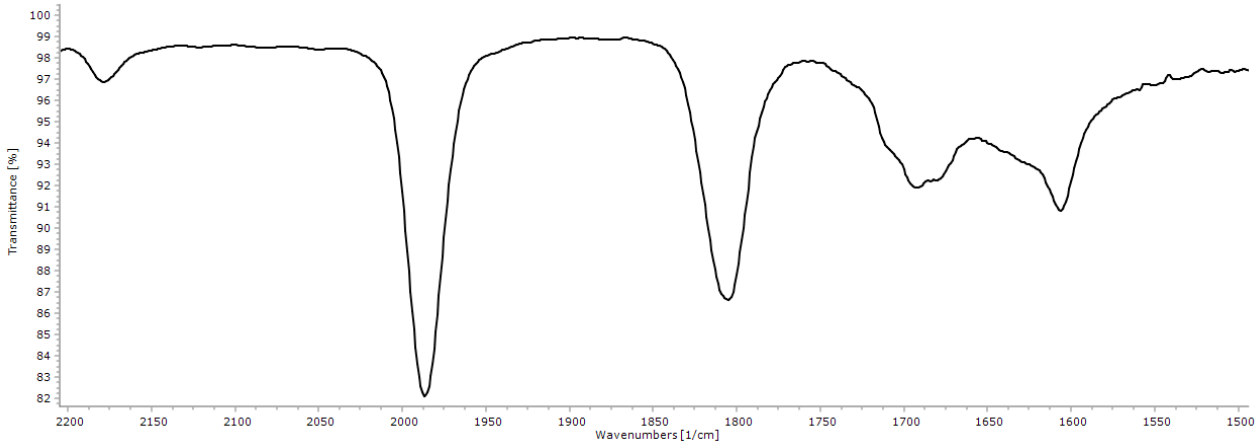

Figure S12. IR spectrum of **[2h]NO_3** in the solid state.

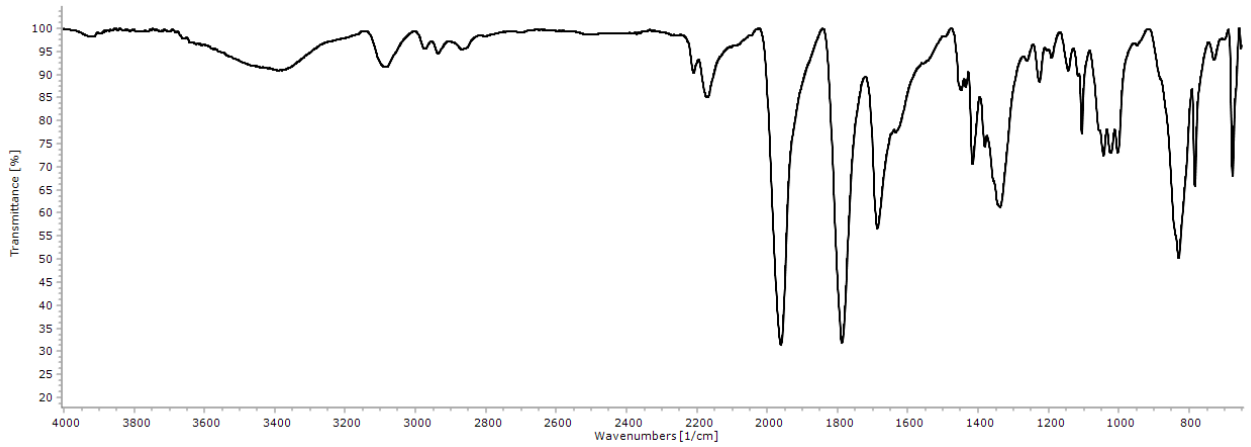

Figure S13. IR spectrum of **3** in CH_2Cl_2 solution.

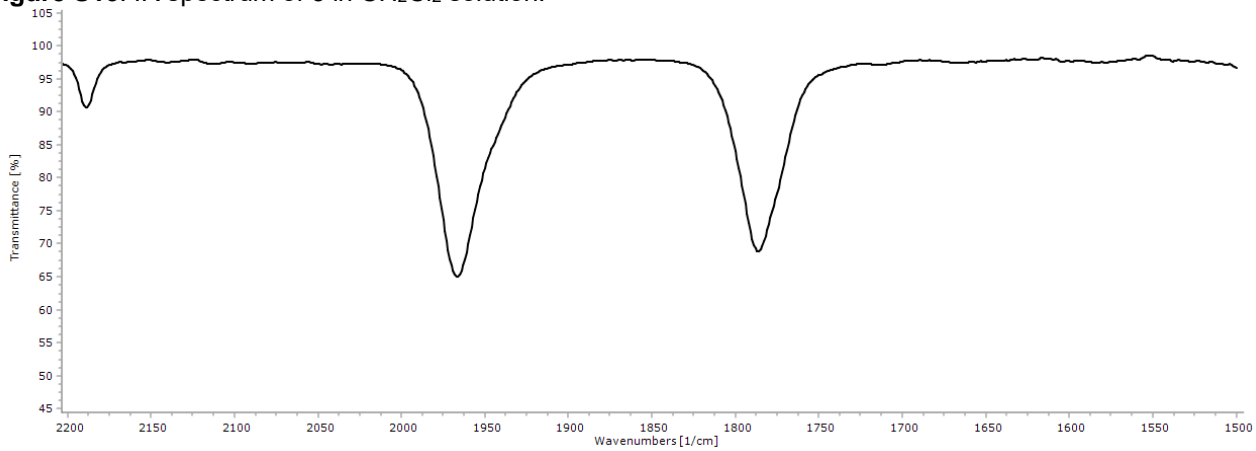

Figure S14. ^{1}H NMR spectrum (401 MHz, acetone-d_6) of **[2a]CF_3SO_3**.

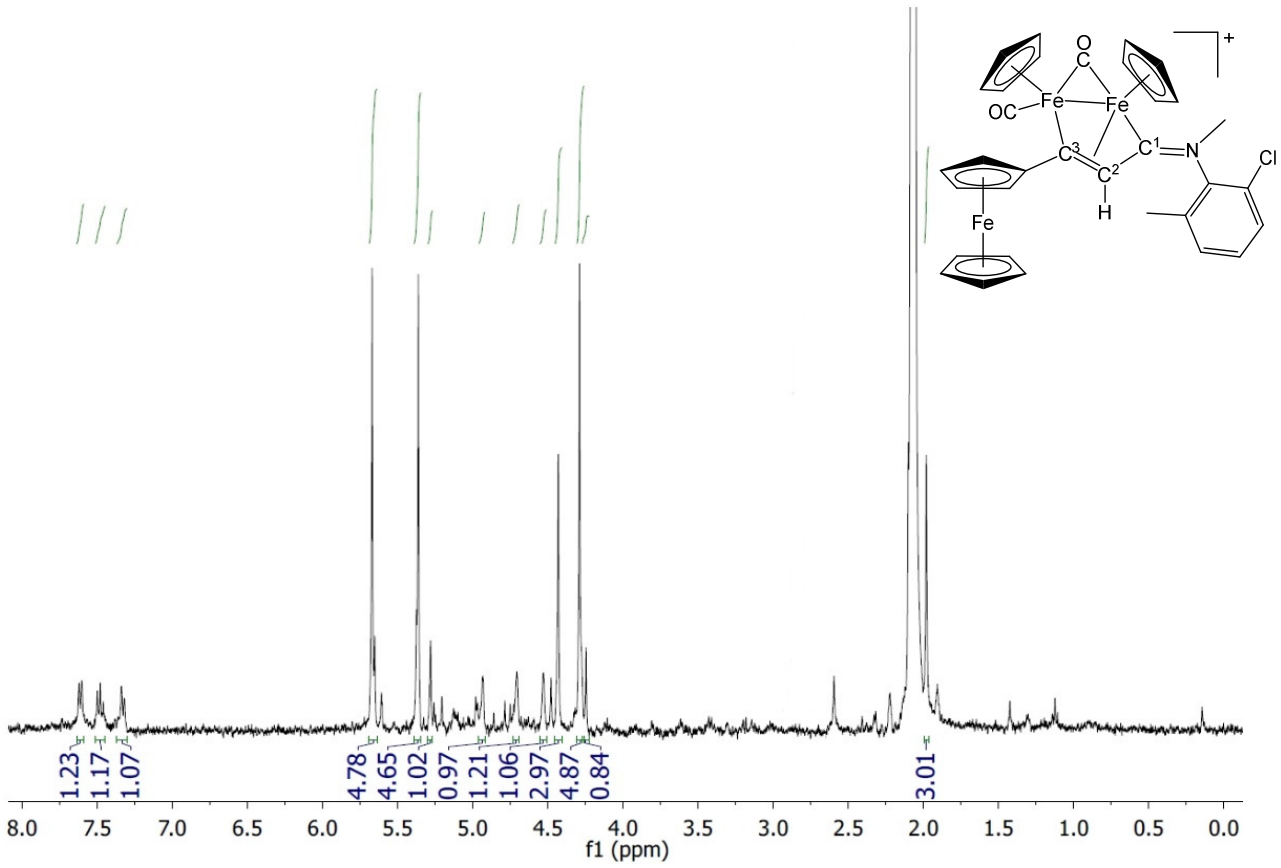

Figure S15. $^{13}C\{^{1}H\}$ NMR spectrum (101 MHz, acetone-d_6) of **[2a]CF_3SO_3**.

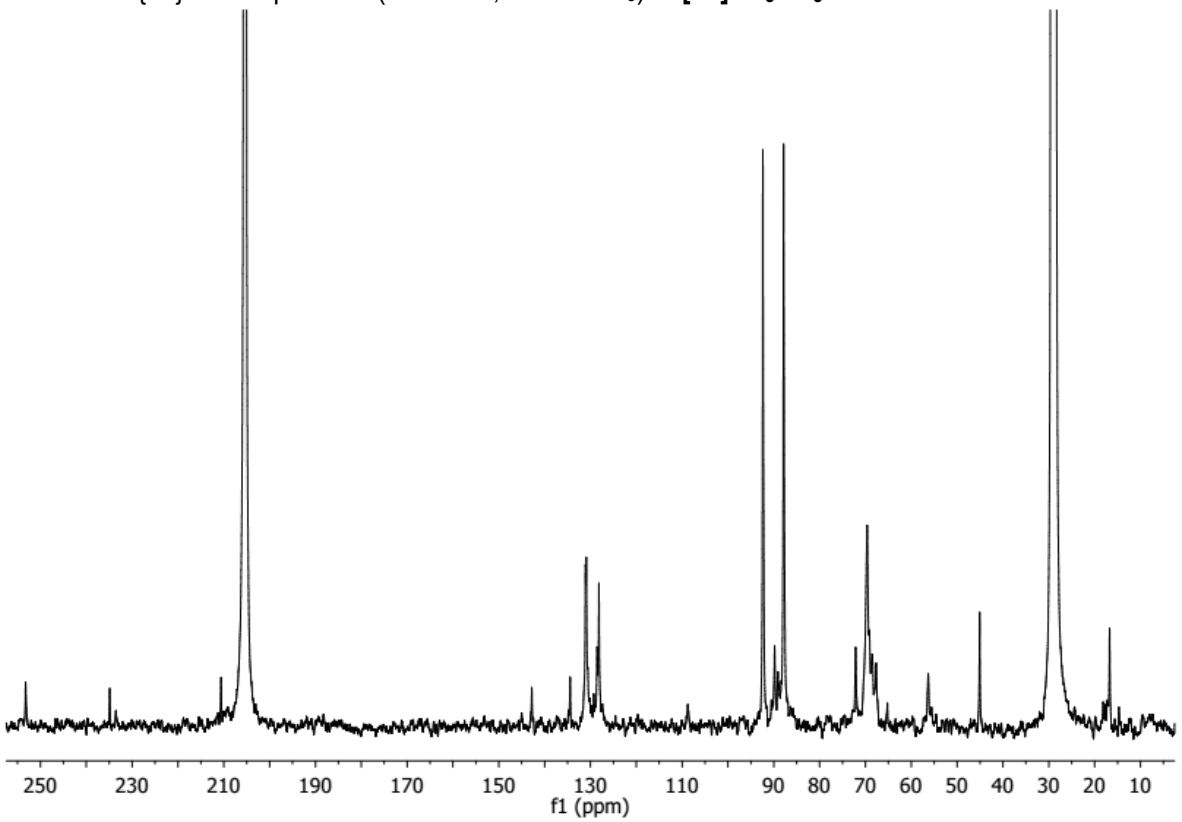

Figure S16. ^{1}H NMR spectrum (401 MHz, acetone-d_6) of **[2b]CF_3SO_3**.

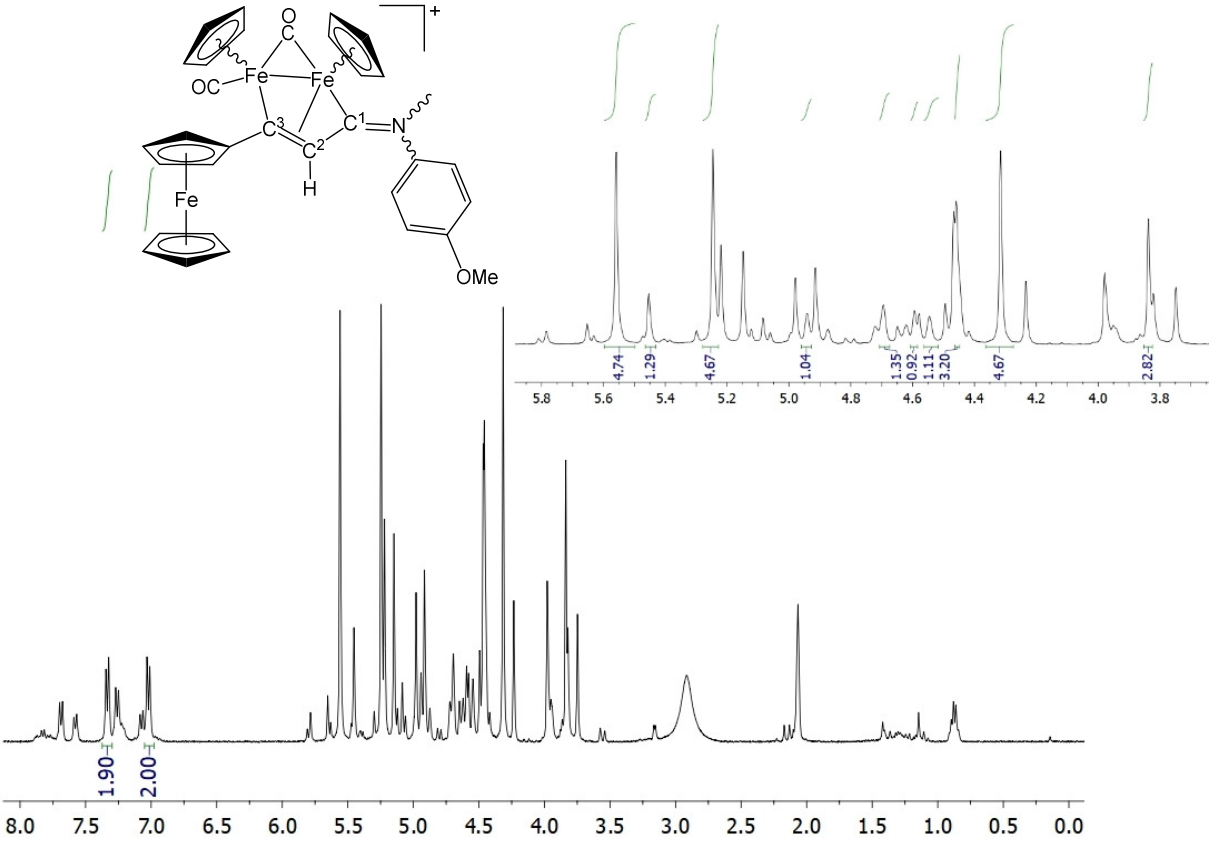

Figure S17. $^{13}C\{^{1}H\}$ NMR spectrum (101 MHz, acetone-d_6) of **[2b]CF_3SO_3**.

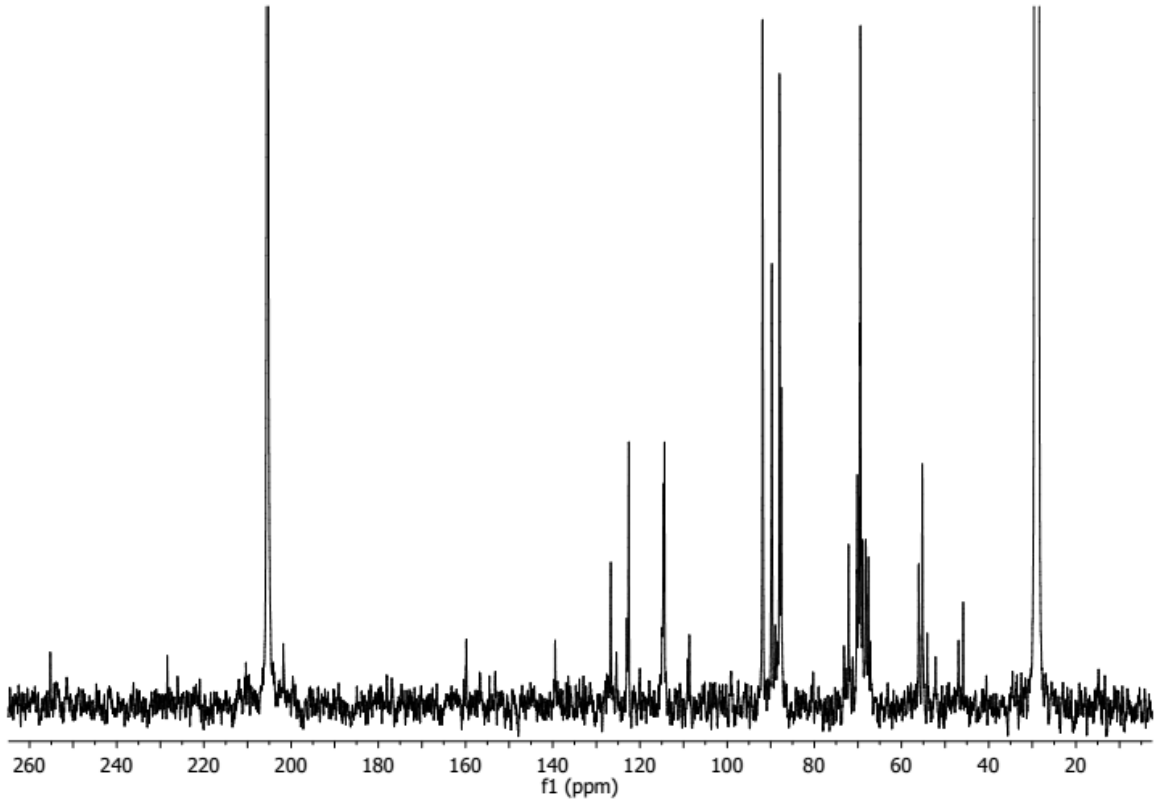

Figure S18. ^{1}H NMR spectrum (401 MHz, acetone-d_6) of **[2c]CF_3SO_3**.

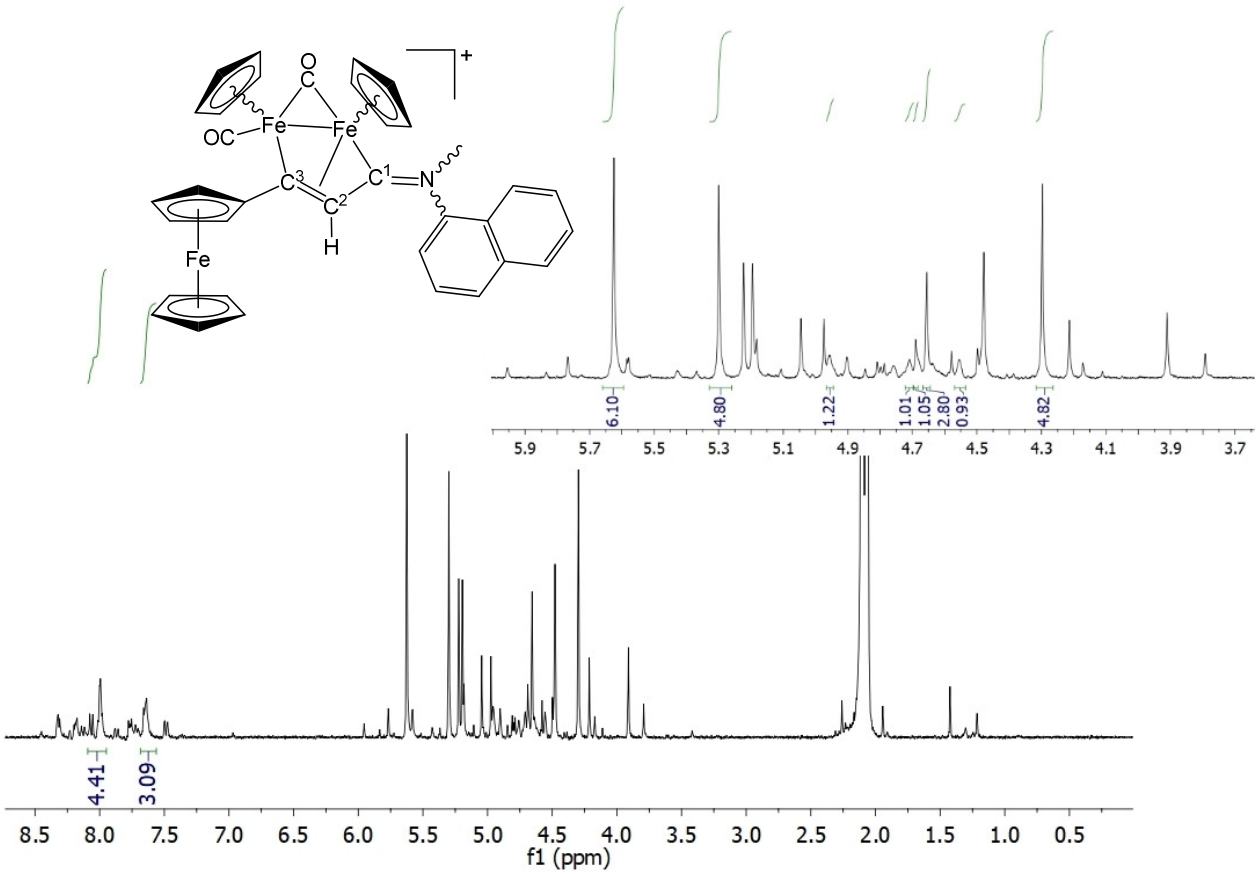

Figure S19. $^{13}C\{^{1}H\}$ NMR spectrum (101 MHz, acetone-d_6) of **[2c]CF_3SO_3**.

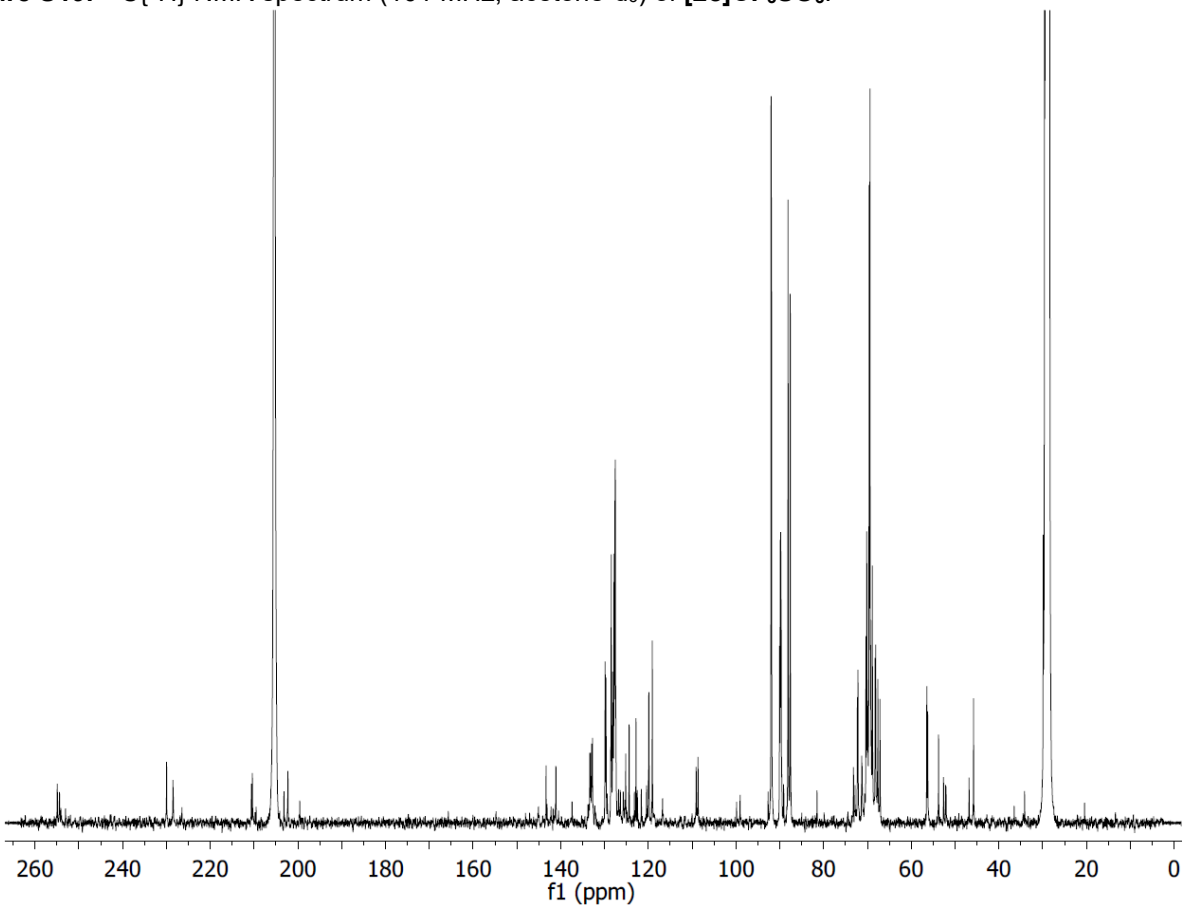

Figure S20. ^{1}H NMR spectrum (401 MHz, acetone-d_6) of **[2d]CF_3SO_3**.

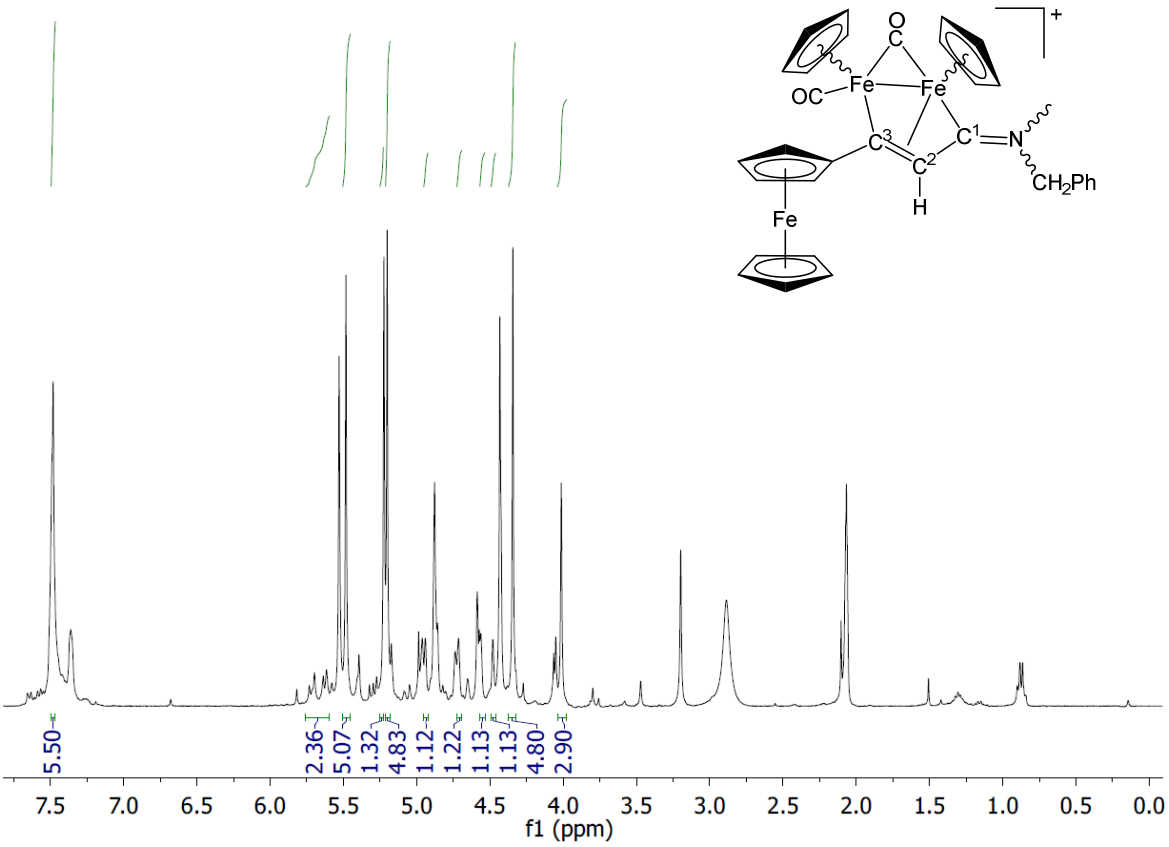

Figure S21. $^{13}C\{^{1}H\}$ NMR spectrum (101 MHz, acetone-d_6) of **[2d]CF_3SO_3**.

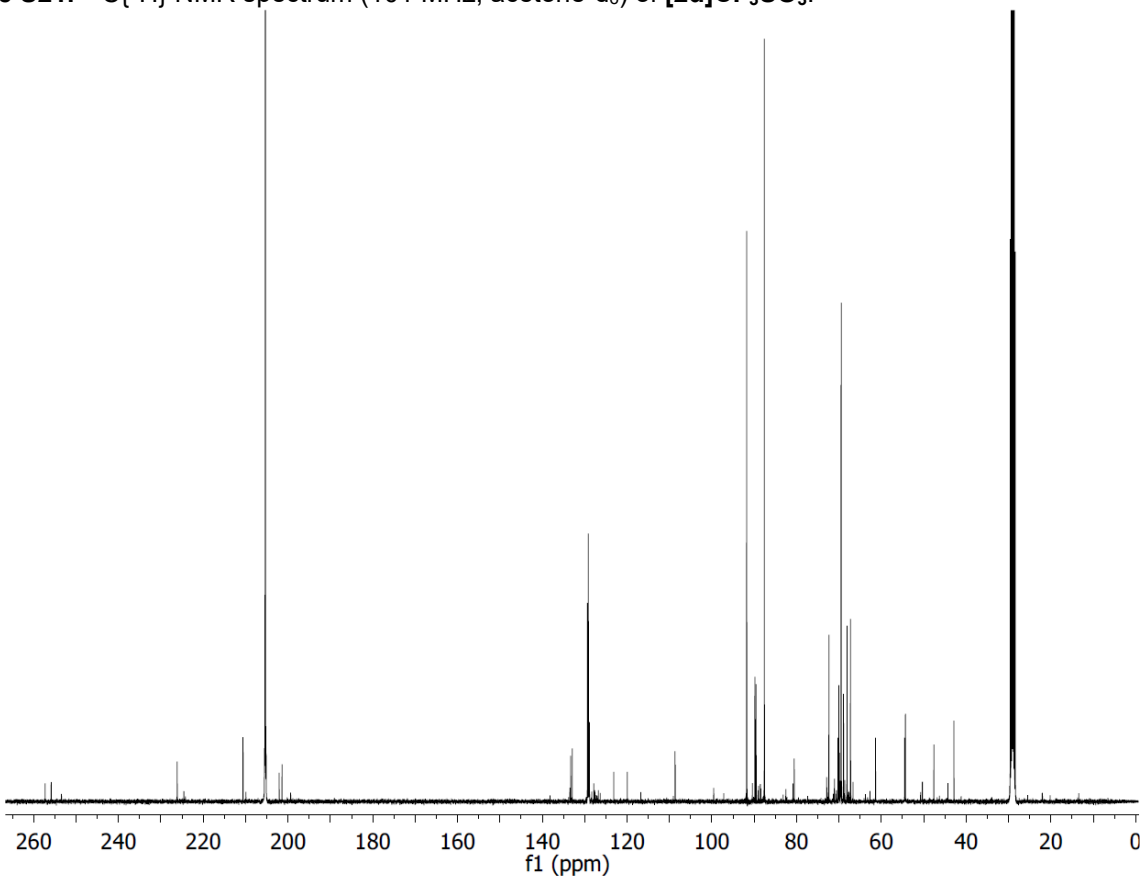

Figure S22. ^{1}H NMR spectrum (401 MHz, acetone-d_6) of **[2e]CF_3SO_3**. Signals due *trans* isomers are marked with asterisk (*) and are not integrated.

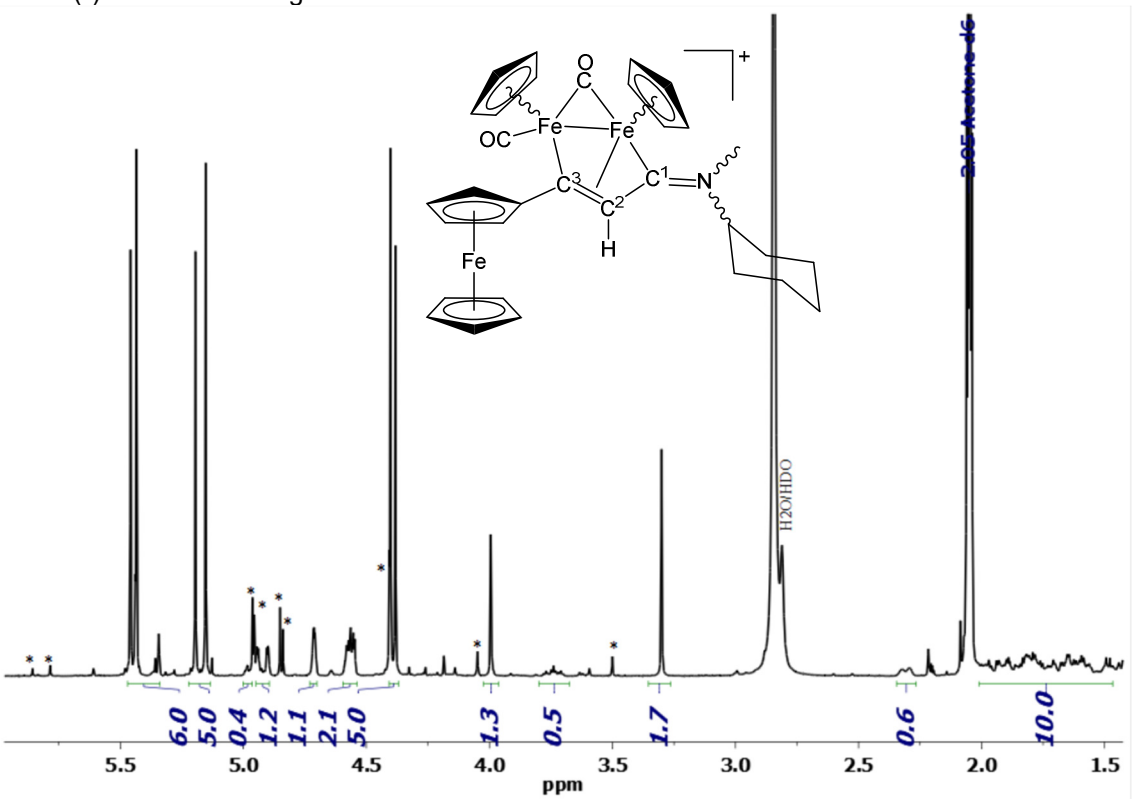

Figure S23. $^{13}C\{^{1}H\}$ NMR spectrum (101 MHz, acetone-d_6) of **[2e]CF_3SO_3**.

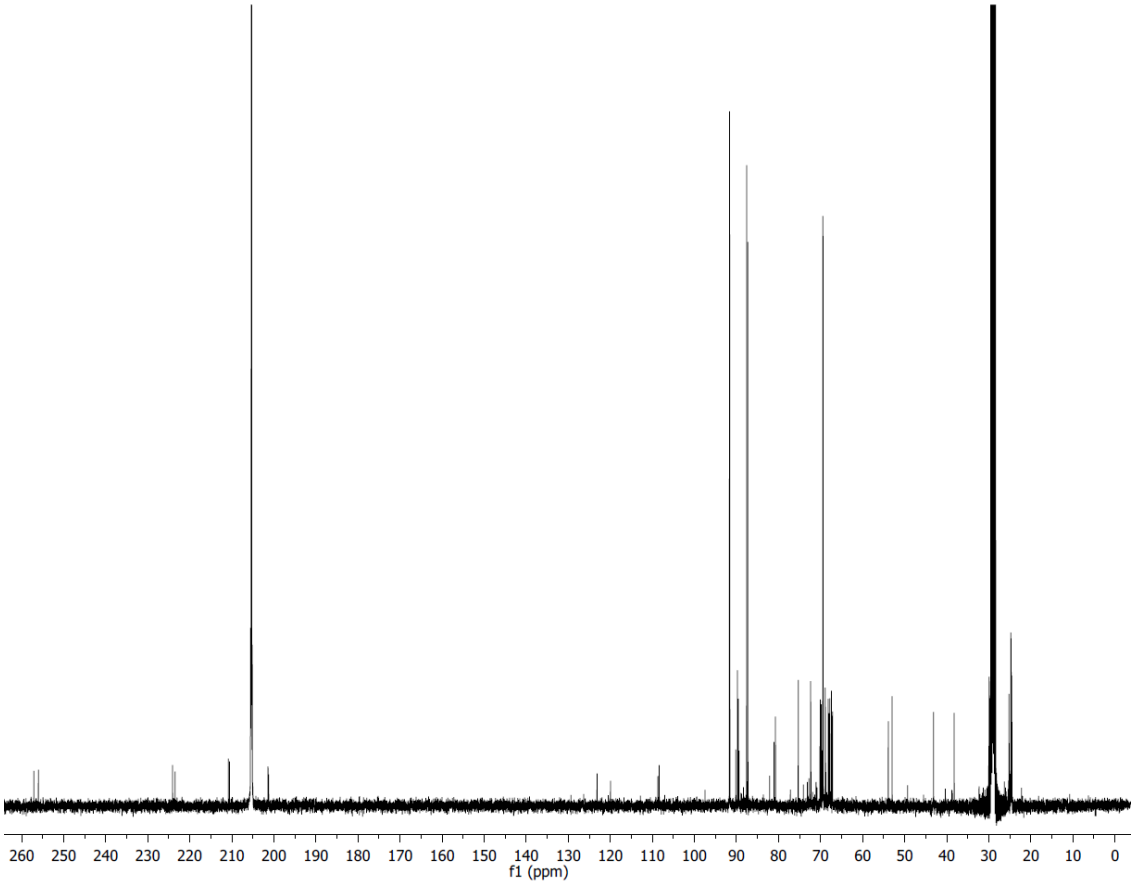

Figure S24. ^{1}H NMR spectrum (401 MHz, acetone-d_6) of **Z-[2e]CF_3SO_3**.

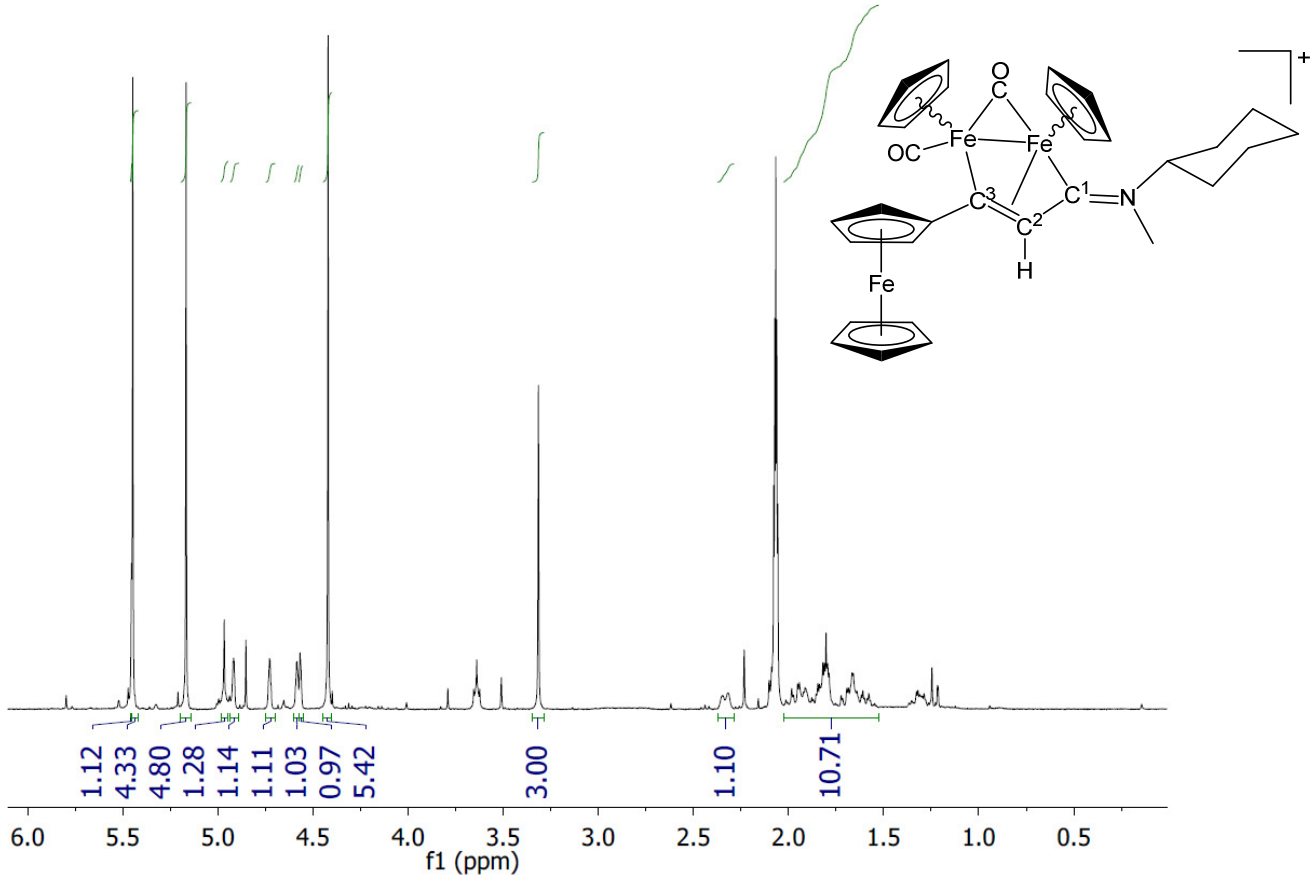

Figure S25. $^{13}C\{^{1}H\}$ NMR spectrum (101 MHz, acetone-d_6) of **Z-[2e]CF_3SO_3**.

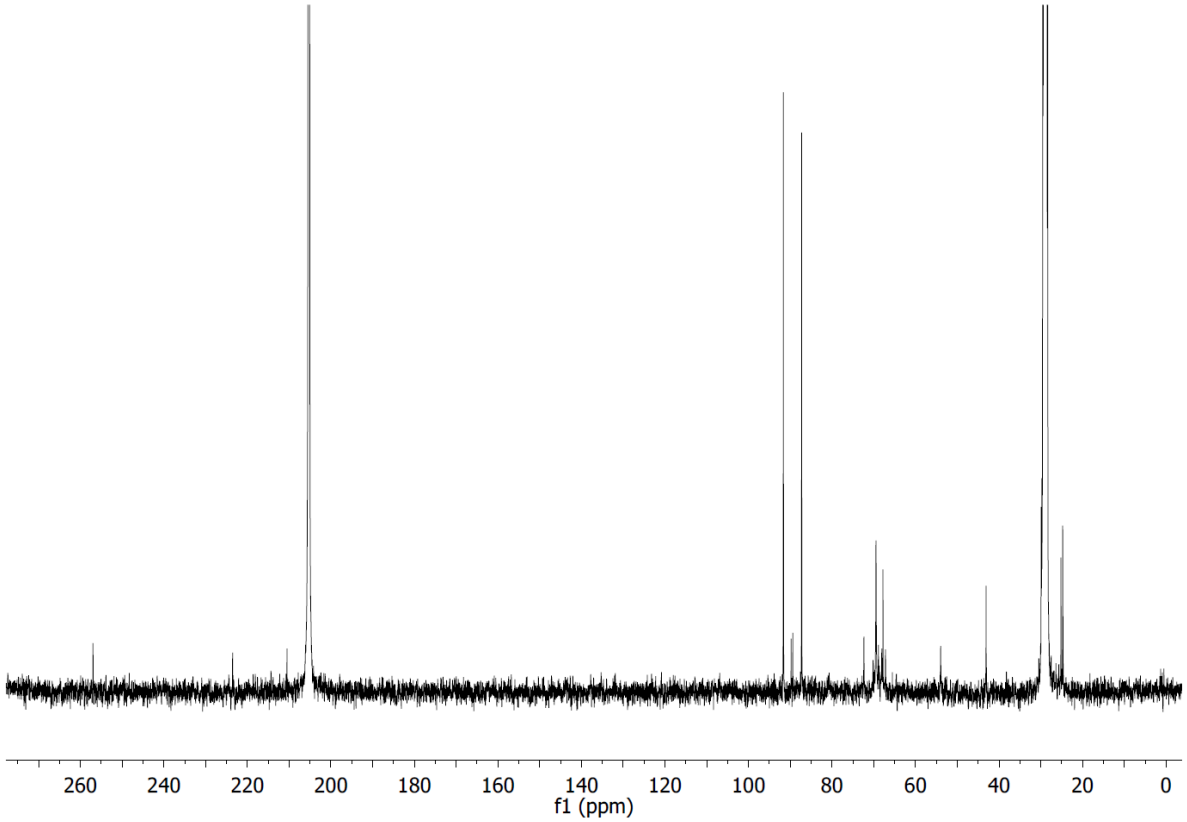

Figure S26. ^{1}H NMR spectrum (401 MHz, acetone-d_6) of **[2f]CF_3SO_3**.

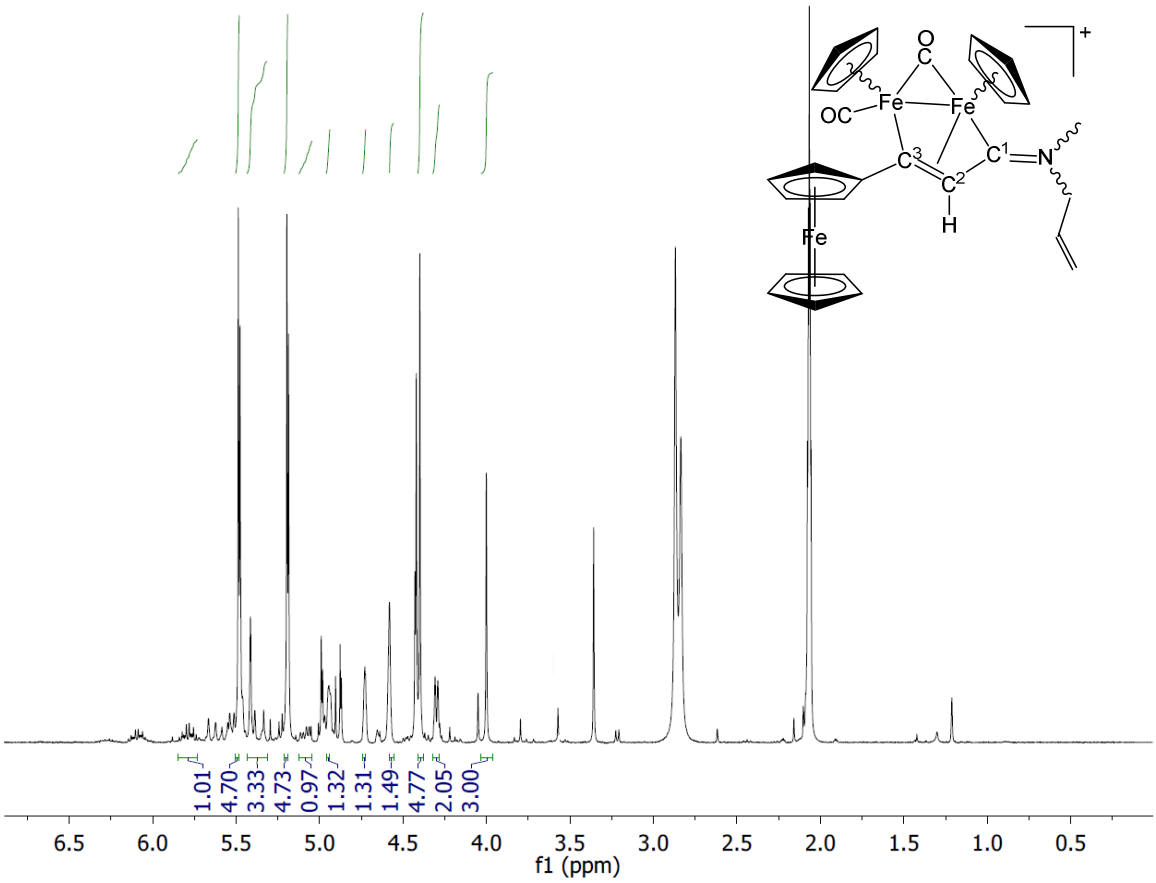

Figure S27. $^{13}C\{^{1}H\}$ NMR spectrum (101 MHz, acetone-d_6) of **[2f]CF_3SO_3**.

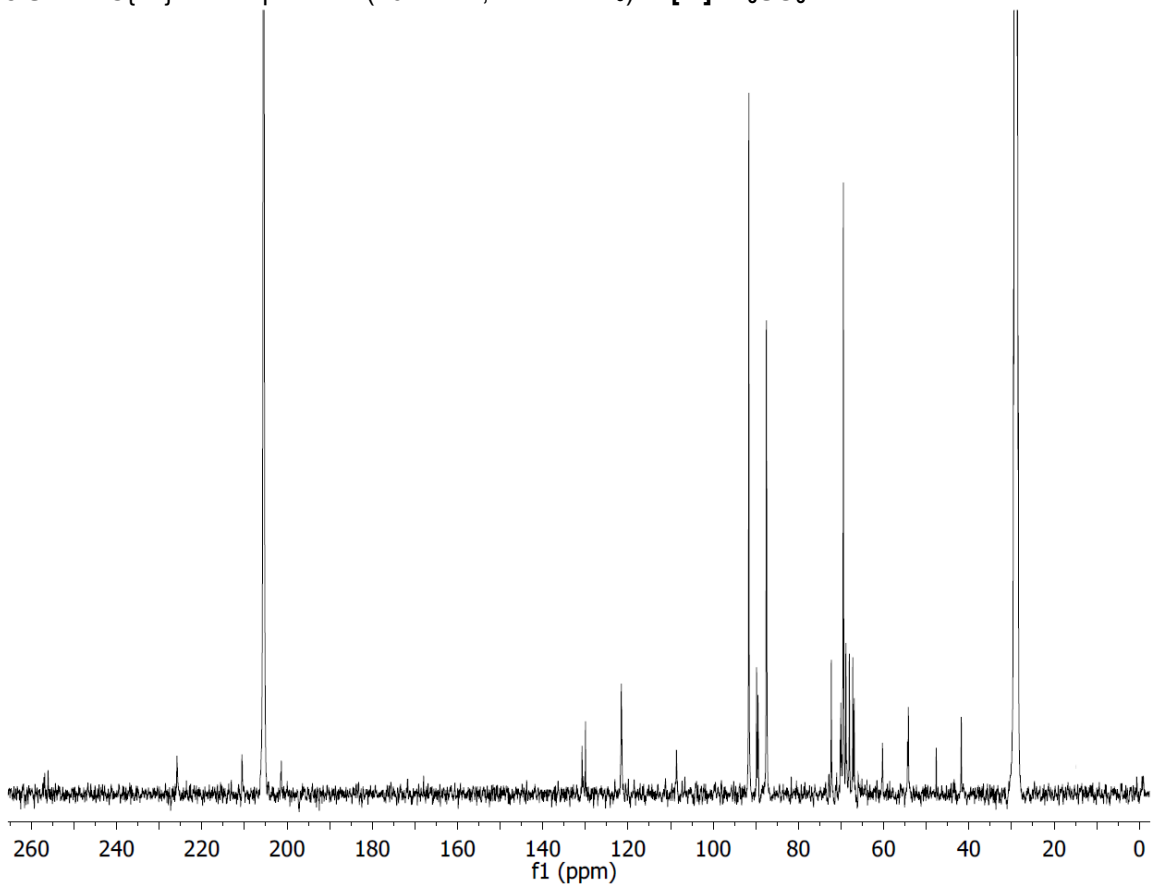

Figure S28. ^{1}H NMR spectrum (401 MHz, acetone-d_6) of **Z-[2f]CF_3SO_3**.

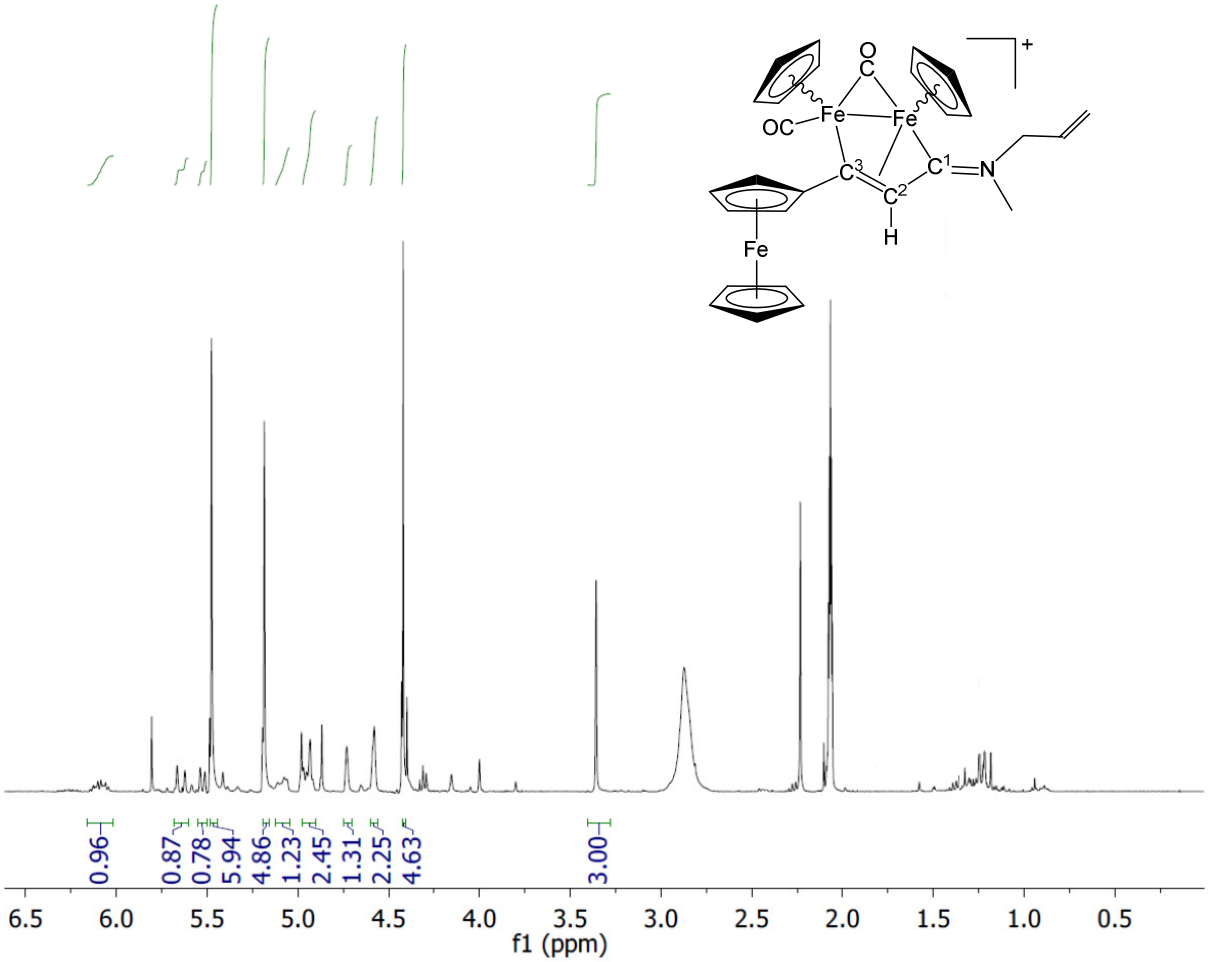

Figure S29. $^{13}C\{^{1}H\}$ NMR spectrum (101 MHz, acetone-d_6) of **Z-[2f]CF_3SO_3**.

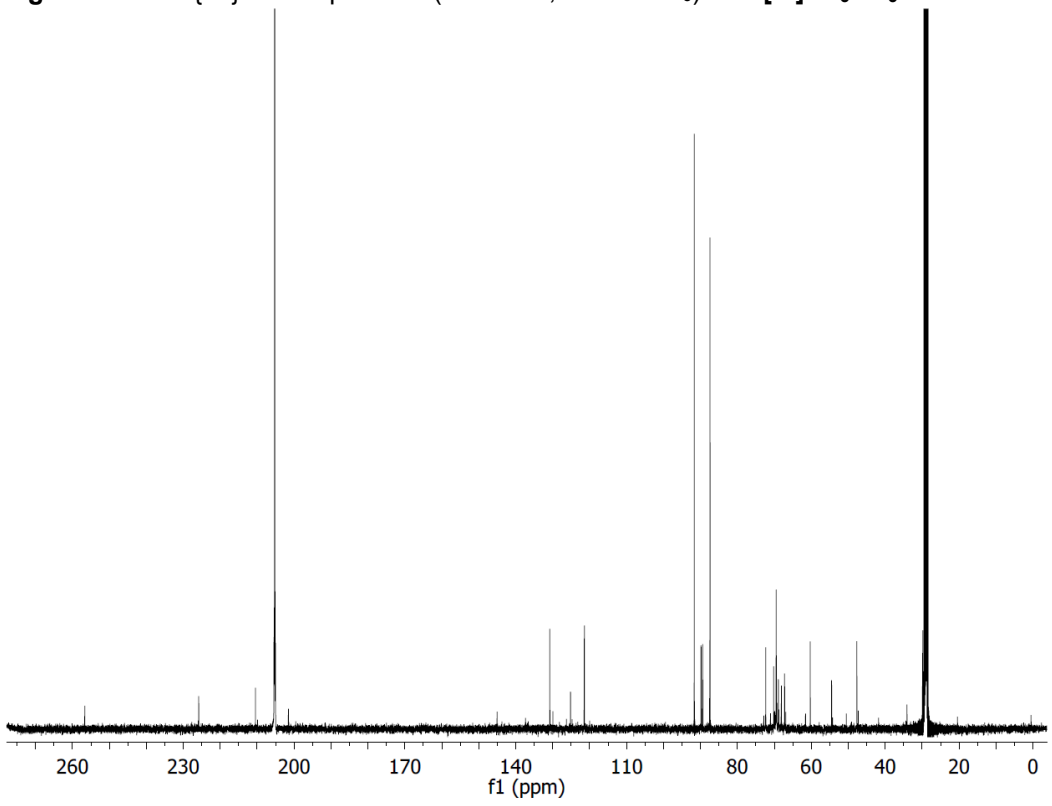

Figure S30. ^{1}H NMR spectrum (401 MHz, acetone-d_6) of **[2g]CF_3SO_3**.

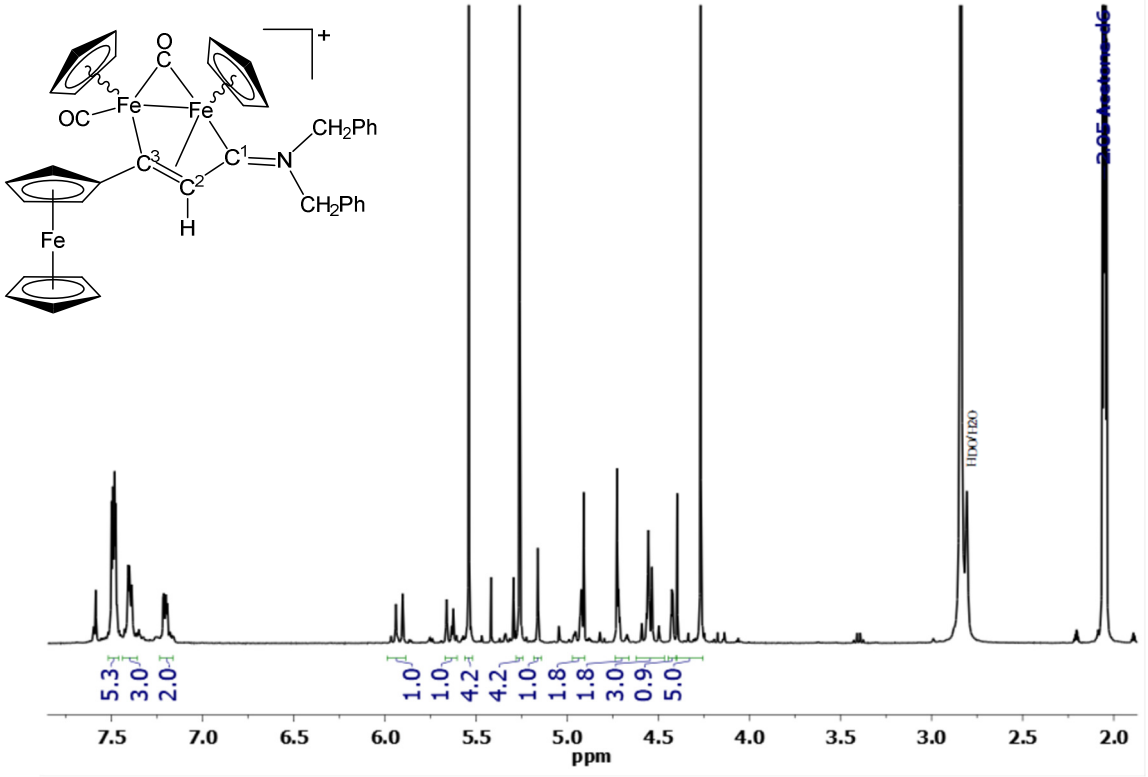

Figure S31. $^{13}C\{^{1}H\}$ NMR spectrum (101 MHz, acetone-d_6) of **[2g]CF_3SO_3**.

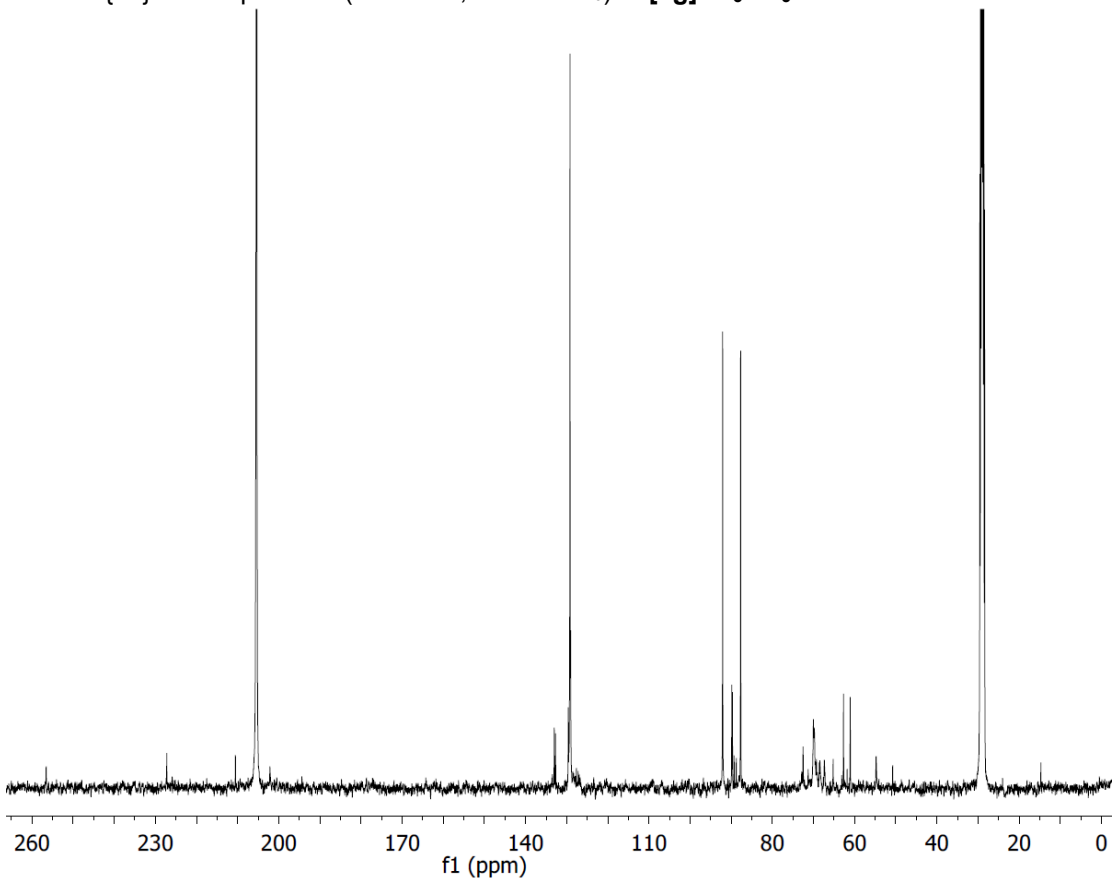

Figure S32. ^{1}H NMR spectrum (401 MHz, acetone-d_6) of **[2h]CF_3SO_3**.

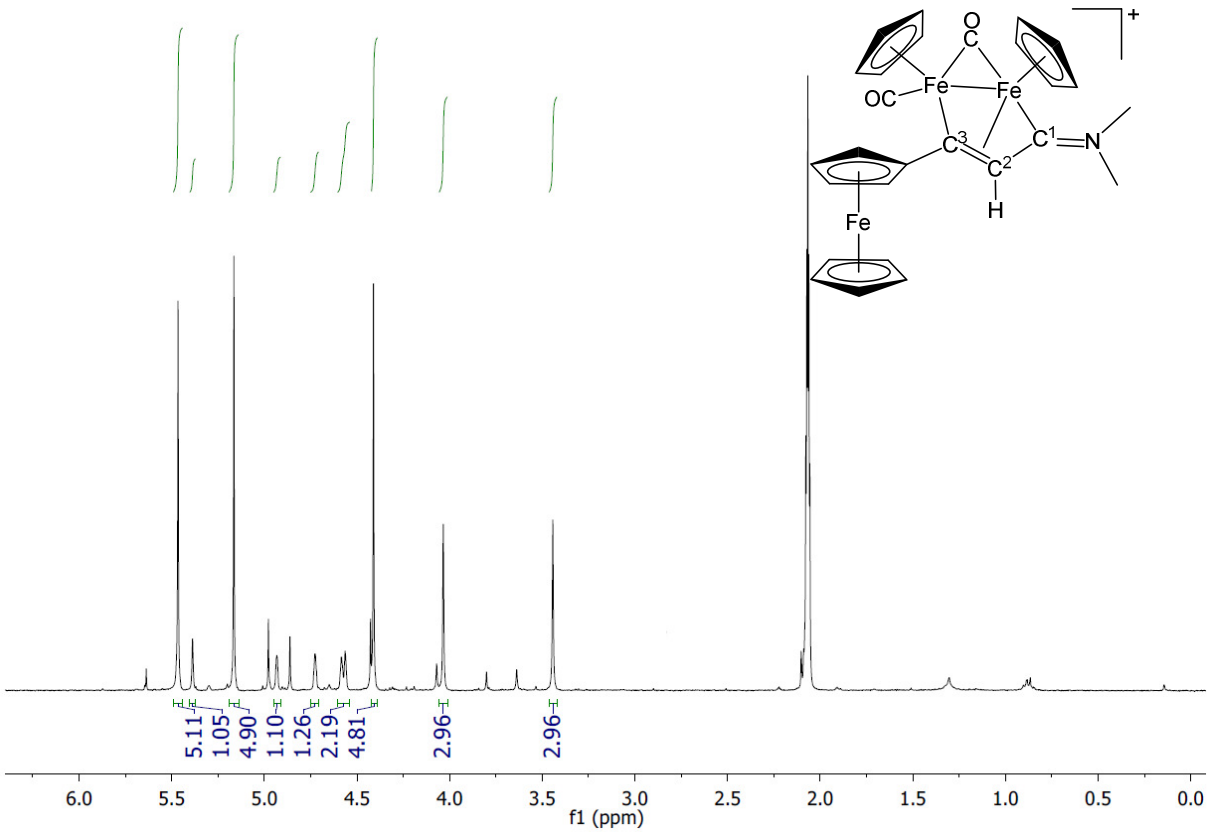

Figure S33. ^{1}H NMR spectrum (401 MHz, acetone-d_6) of [**2i**]CF_3SO_3.

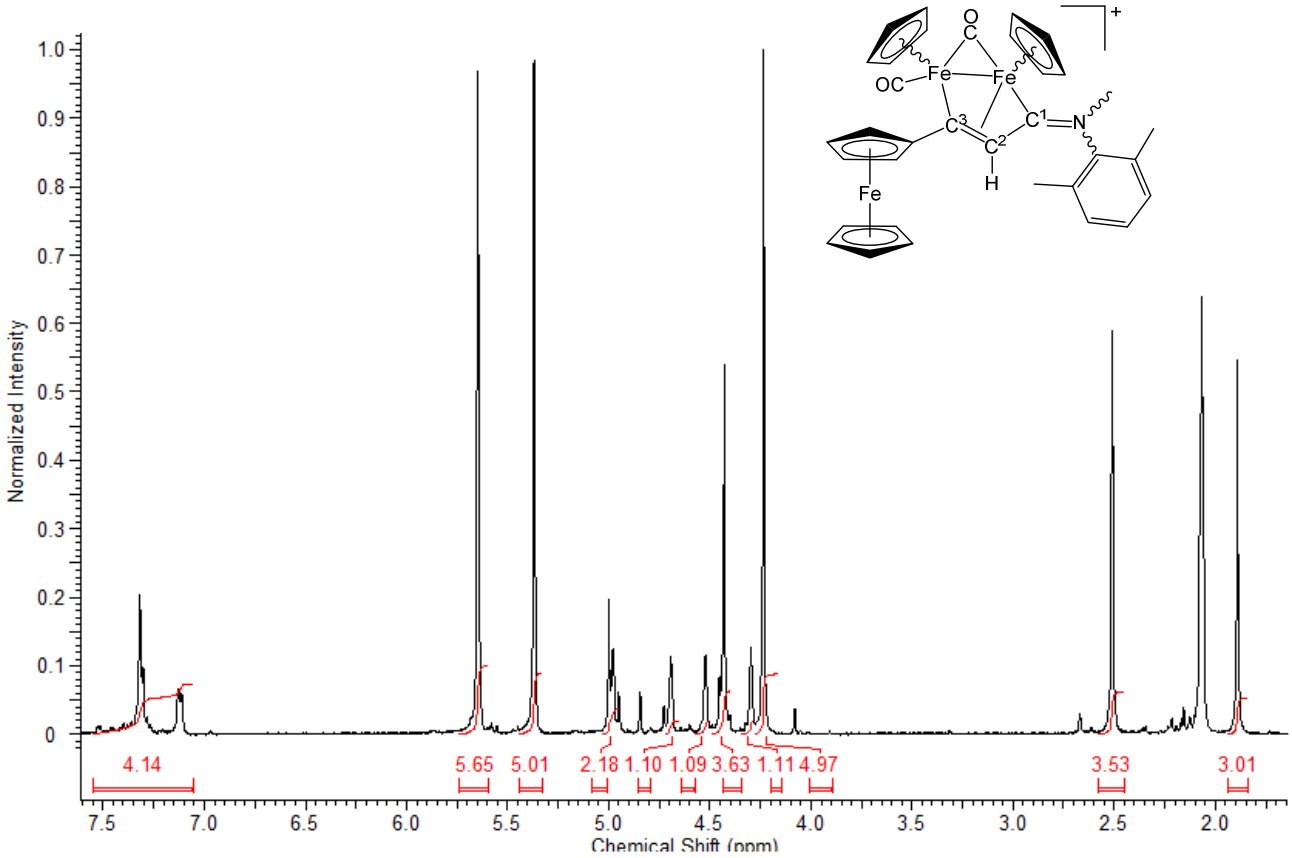

Figure S34. ^{1}H NMR spectrum (401 MHz, acetone-d_6) of **[2h]NO_3**.

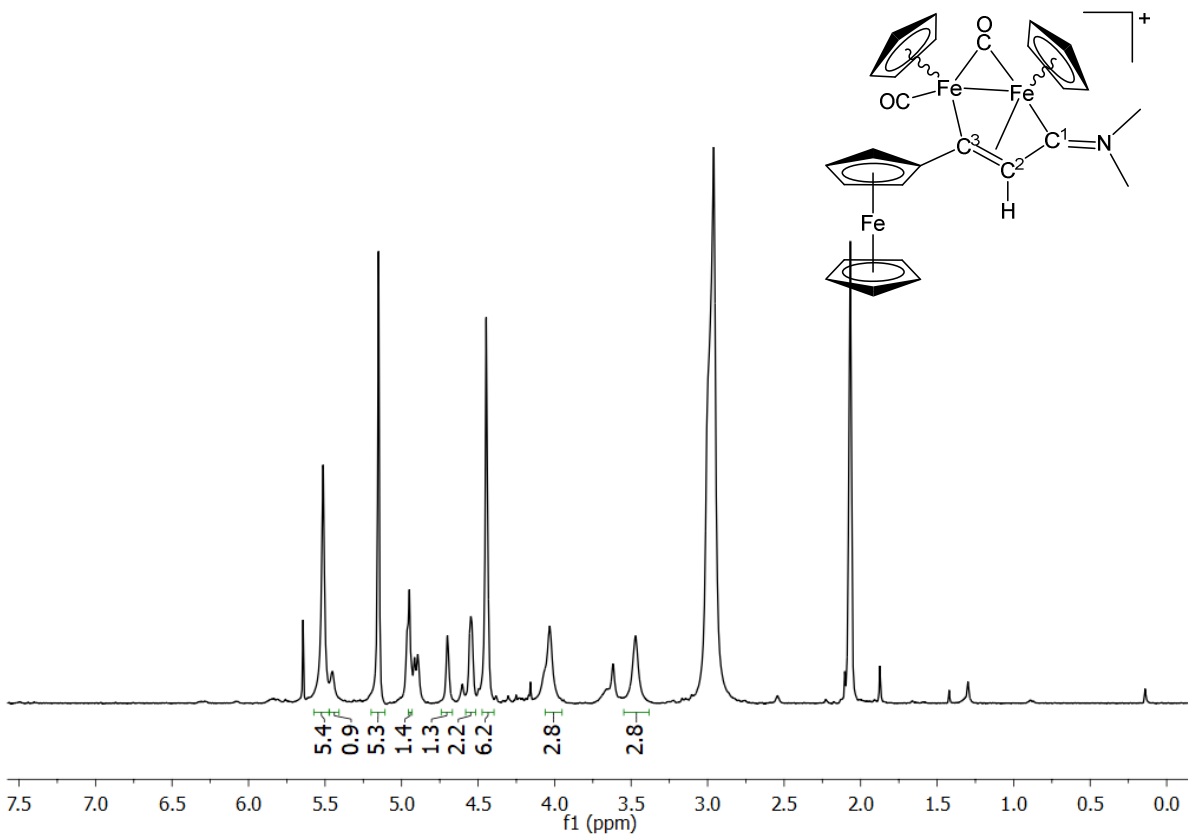

Figure S35. ^{14}N NMR spectrum (29 MHz, acetone-d_6) of **[2h]NO_3**.

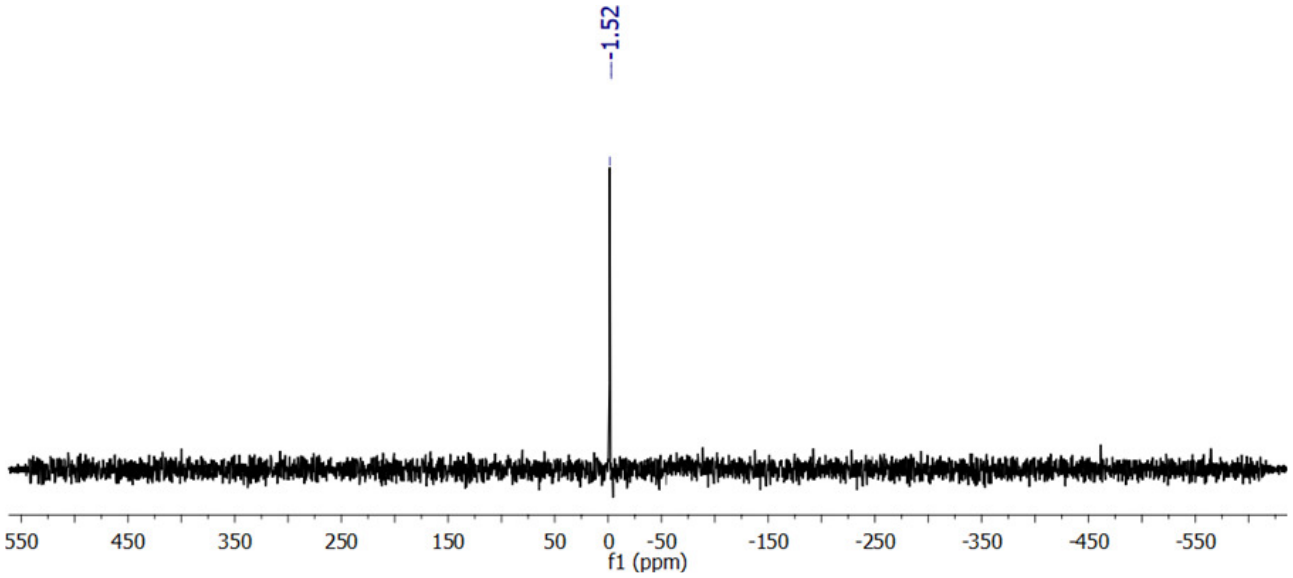

Figure S36. ^{1}H NMR spectrum (401 MHz, acetone-d_6) of **3**.

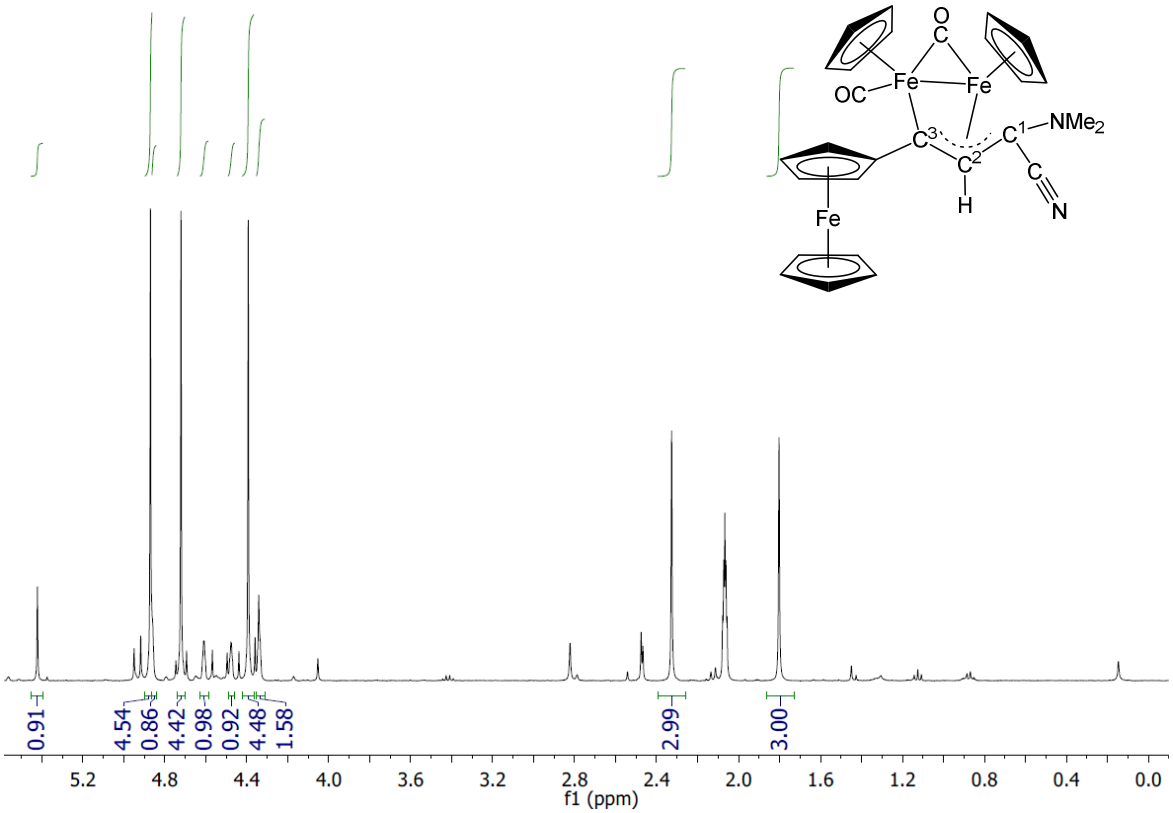

Figure S37. $^{13}C\{^{1}H\}$ NMR spectrum (101 MHz, acetone-d_6) of **3**.

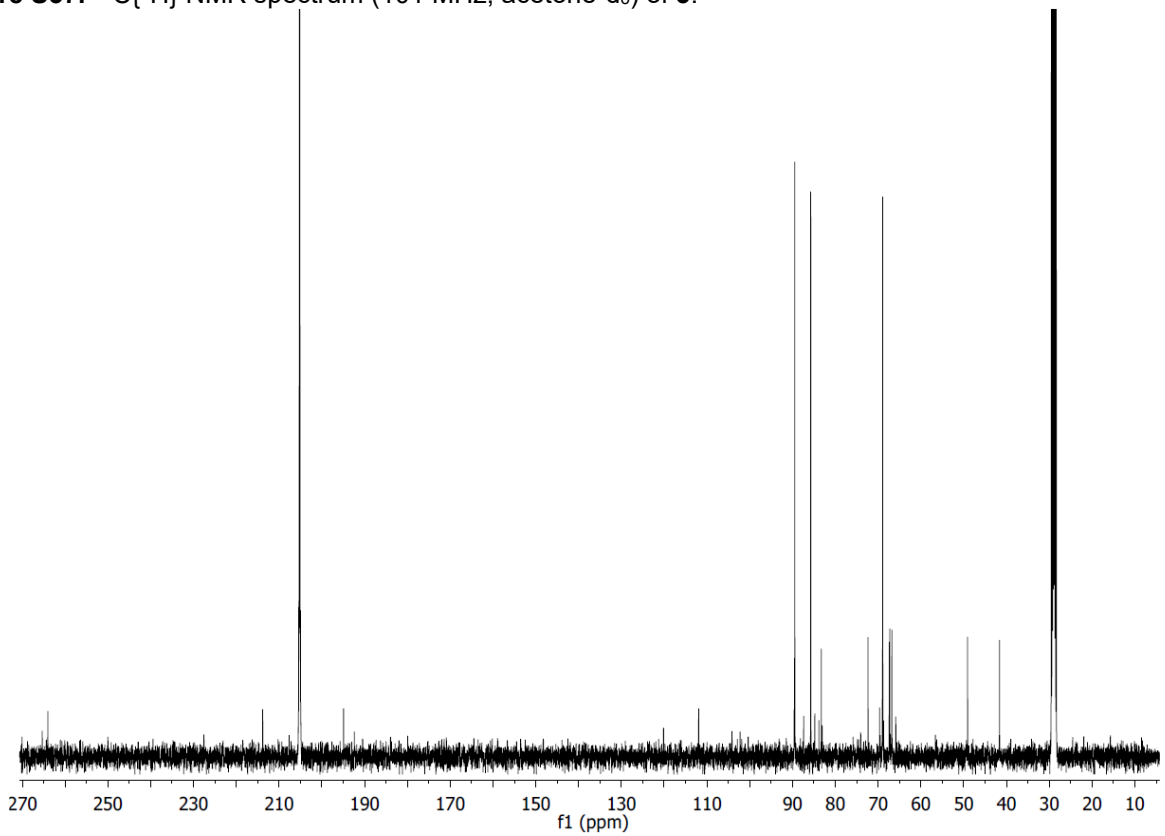

Figure S38. ^{1}H NMR spectrum (401 MHz, acetone-d_6) of **4**.

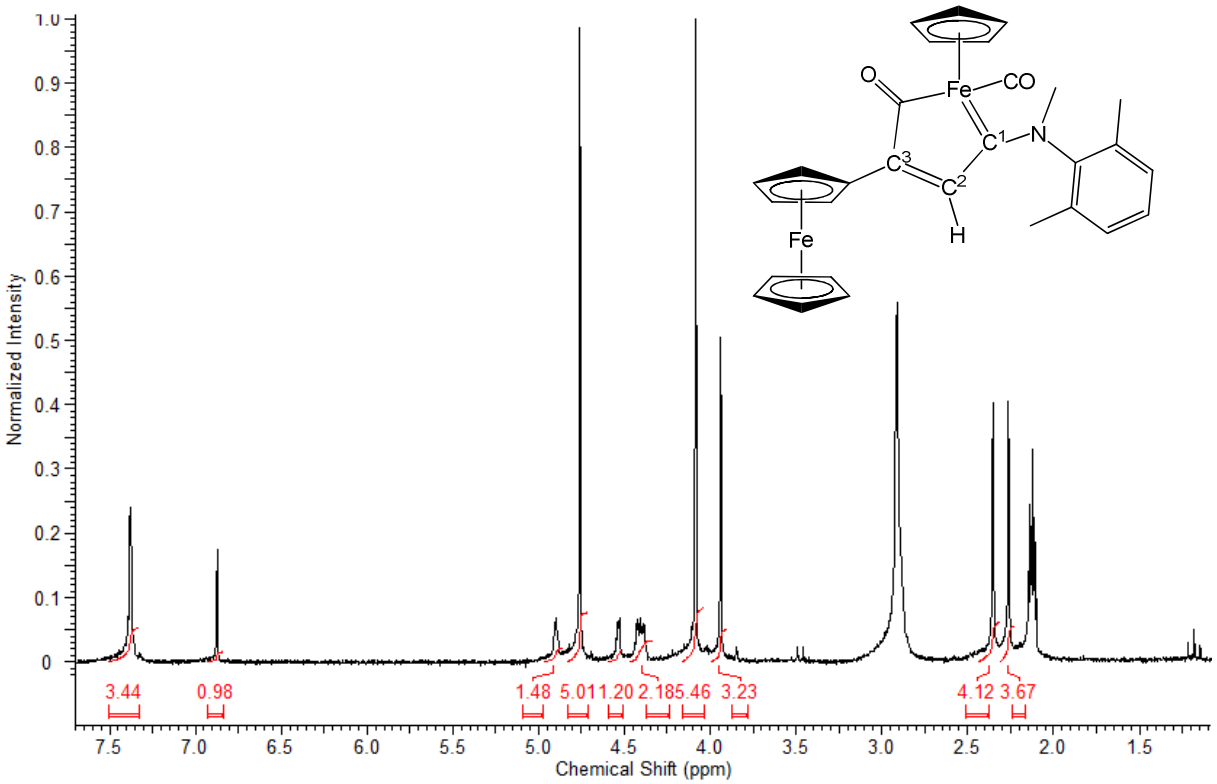

Figure S39. ^{1}H (black line) and ^{1}H-NOESY (red line: irradiation at 5.26 ppm; blue line: irradiation at 5.54 ppm) NMR spectra (401 MHz, acetone-d_6) of ***cis*-[2g]CF_3SO_3**. Below: structure of ***cis*-[2g]$^+$** with NOE effects represented by red/blue arrows and selected ^{1}H NMR chemical shifts (ppm) next to each group.

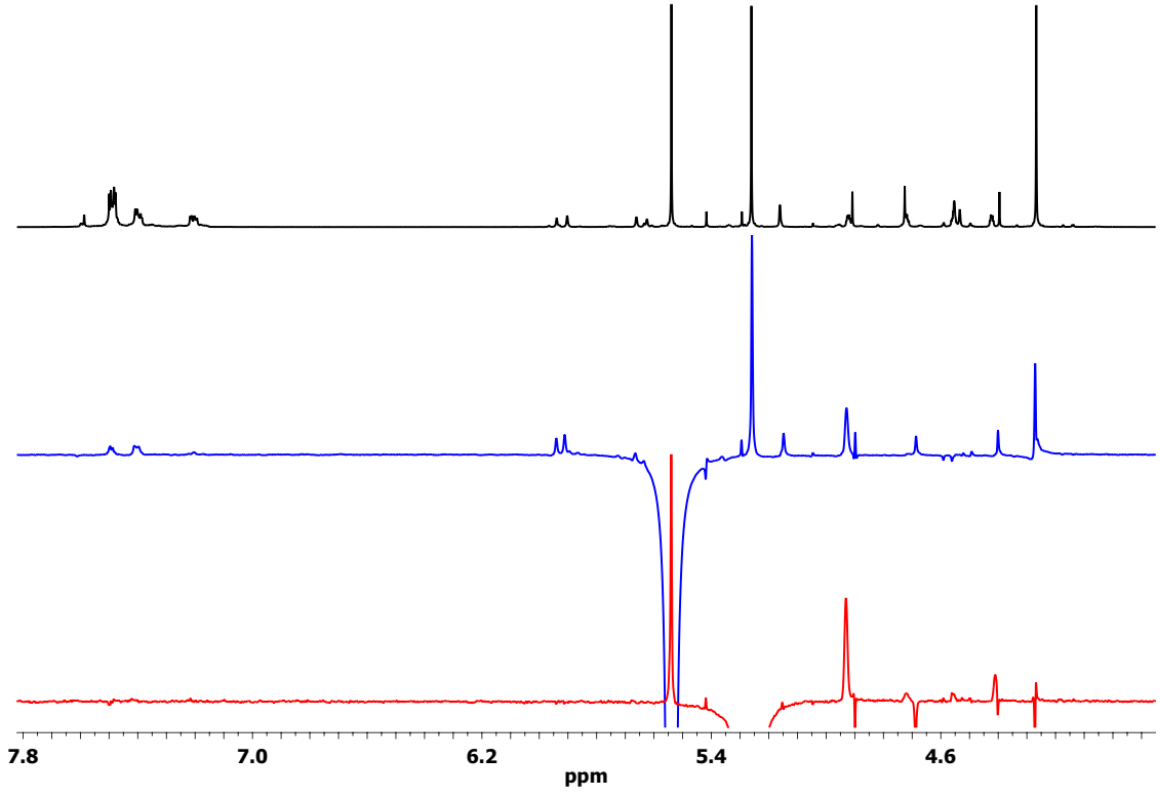

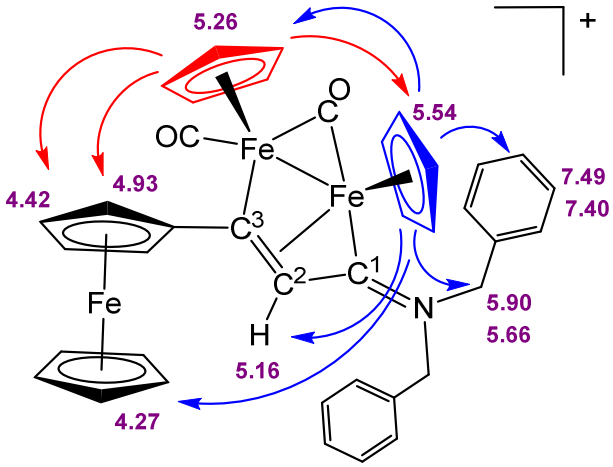

Figure S40. ^{1}H (black line) and ^{1}H-NOESY (red line: irradiation at 5.19 ppm; blue line: irradiation at 3.99 ppm) NMR spectra (401 MHz, acetone-d_6) of ***cis-E*-[2e]CF_3SO_3**. Below: structure of ***cis-E*-[2e]$^+$**; substituents with the highest priority around the C=N double bond are highlighted in green. NOE effects are represented by red/blue arrows and selected ^{1}H NMR chemical shifts (ppm) are reported next to each group.

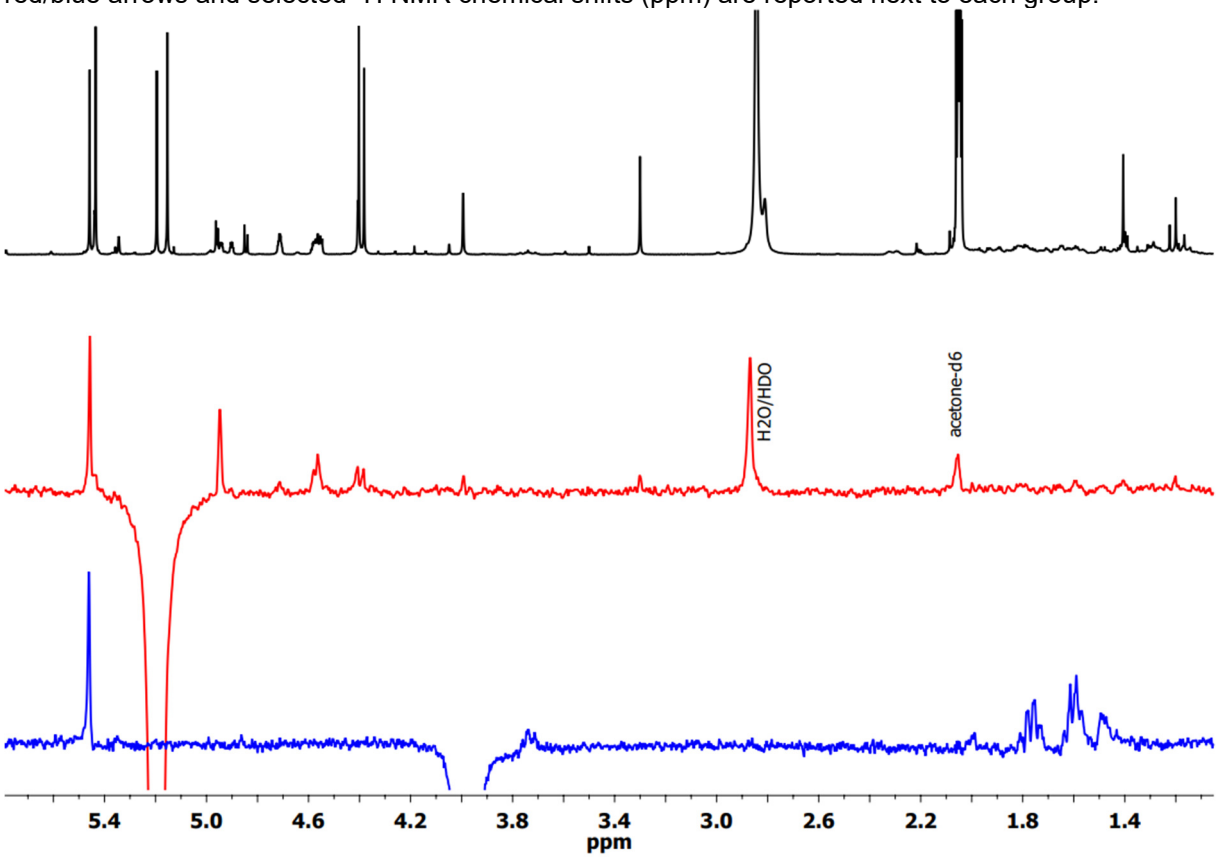

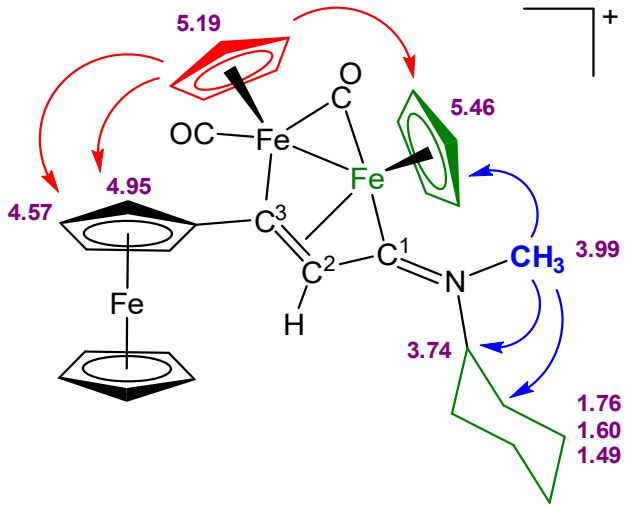

Figure S41. ^{1}H (black line) and ^{1}H-NOESY (red line: irradiation at 5.19 ppm; blue line: irradiation at 3.99 ppm) NMR spectra (401 MHz, acetone-d_6) of ***cis-Z*-[2e]CF_3SO_3**. Below: structure of ***cis-Z*-[2e]$^+$**; substituents with the highest priority around the C=N double bond are highlighted in green. NOE effects are represented by red/blue arrows and selected ^{1}H NMR chemical shifts (ppm) are reported next to each group.

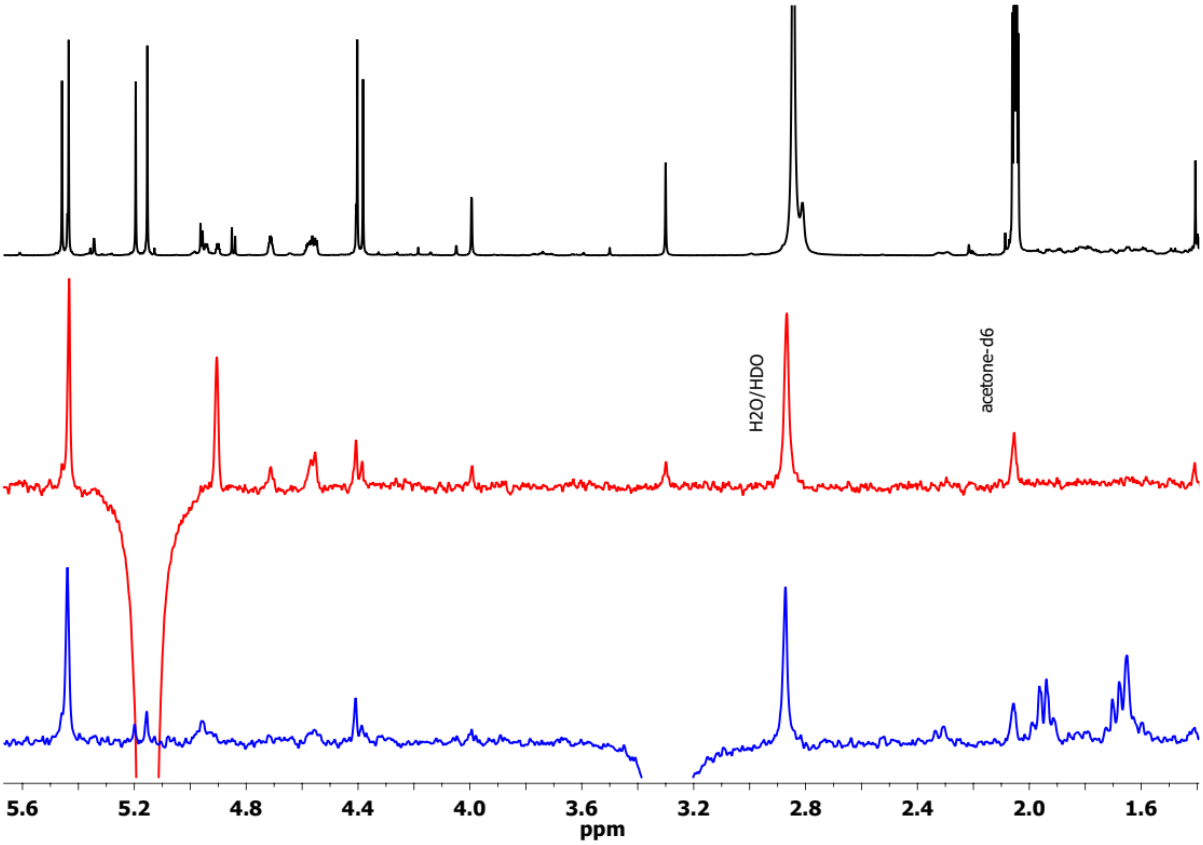

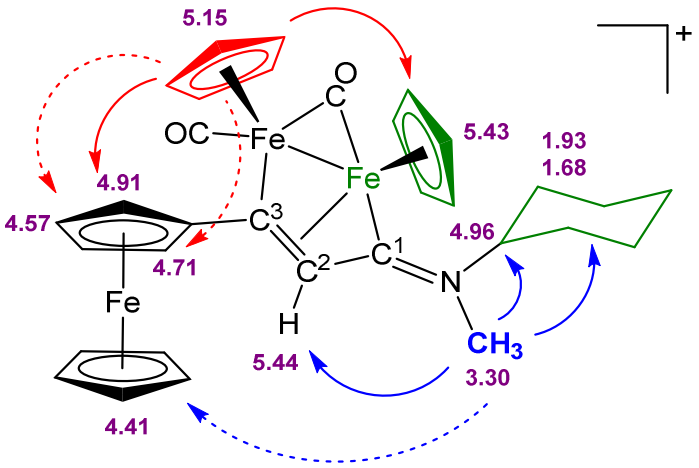

NMR data of complexes in D_2O/CD_3OD mixtures

[**2a**]CF_3SO_3. ^1H NMR (CD_3OD/D_2O = 1:1): δ/ppm = 7.39, 7.27, 7.12 (m, 3 H, C_6H_3); 5.33, *5.30*, *5.08*, 5.07 (s, 10 H, Cp); 5.03 (s, 1 H, C^2H); 4.14 (s, 3 H, NMe); 4.11 (s, 5 H, Cp^{Fc}); 1.77 (s, 3 H, C_6H_3*Me*).

[**2b**]CF_3SO_3. ^1H NMR (CD_3OD/D_2O = 1:1): δ/ppm = *7.42*, *7.12*, 7.03, 6.87 (d, ^3J = 8.7 Hz, 4 H, C_6H_4); 5.23, 5.01 (s, 10 H, Cp); 5.10 (s, 1 H, C^2H); 4.20 (s, 3 H, NMe); 4.13 (s, 5 H, Cp^{Fc}); 3.69 (s, 3 H, OMe).

[**2c**]CF_3SO_3. ^1H NMR (CD_3OD/D_2O = 1:1): δ/ppm = 8.30-7.00 (m, 7 H, $C_{10}H_7$); 5.27, 5.03, *4.92*, *4.89* (s, 10 H, Cp); 4.32 (s, 3 H, NMe); 4.08 (s, 5 H, Cp^{Fc}).

[**2d**]CF_3SO_3. ^1H NMR (CD_3OD/D_2O = 1:1): δ/ppm = 7.50-7.10 (m, 5 H, Ph); 5.49, 5.32 (d, $^2J_{HH}$ = 14 Hz, 2 H, CH_2); *5.18*, 5.15, *4.98*, 4.92 (s, 10 H, Cp); *4.27*, 4.07 (s, 5 H, Cp^{Fc}); 3.90 (s, 3 H, NMe).

[**2e**]CF_3SO_3. ^1H NMR (CD_3OD/D_2O = 1:1): δ/ppm = 5.14, *5.12*, 4.96, *4.91* (s, 10 H, Cp); *5.02*, 5.00 (s, 1 H, C^2H); 4.49, 4.47, 4.37, 4.27 (m, 4 H, C_5H_4); *4.26*, 4.24 (s, 5 H, Cp^{Fc}); 3.74, *3.07* (s, 3 H, NMe); 3.35 (m, 1 H, CH^{Cy}); 2.10-0.90 (m, 10 H, CH_2^{Cy}).

[**2f**]CF_3SO_3. ^1H NMR (CD_3OD/D_2O = 1:1): δ/ppm = 5.72 (m, 1 H, C*H*=CH_2); 5.40, 5.26 (m, 2 H, CH=C*H*$_2$); 5.16, *5.15*, 4.94, *4.93* (s, 10 H, Cp); *4.26*, 4.23 (s, 5 H, Cp^{Fc}); 3.77 (s, 3 H, NMe).

[**2g**]CF_3SO_3. ^1H NMR (CD_3OD/D_2O = 1:1): δ/ppm = 7.50-6.90 (m, 10 H, Ph); 5.68, 5.49 (d, $^2J_{HH}$ = 14.4 Hz, 2 H, CH_2); 5.19, 5.98 (s, 10 H, Cp); 4.42, 4.13, 4.12, 4.09 (m, 4 H, C_5H_4); 4.32 (s, 1 H, C^2H); 4.04 (s, 5 H, Cp^{Fc}).

[**2h**]CF_3SO_3. ^1H NMR (CD_3OD/D_2O = 1:1): δ/ppm = 5.15, 4.91, *4.70* (s, 10 H, Cp); 5.00 (s, 1 H, C^2H); 4.46, 4.37 (m, 4 H, C_5H_4); *4.27*, 4.25 (s, 5 H, Cp^{Fc}); *3.78*, 3.77, *3.32*, 3.18 (s, 6 H, NMe_2).

[**2i**]CF_3SO_3. ^1H NMR (CD_3OD/D_2O = 1:1): δ/ppm = 7.41–7.26, 7.15–7.04 (m, 3 H, C_6H_3); 5.47, 5.24 (s, 10 H, Cp); 4.74, 4.56, 4.26 (s, 3 H, C_5H_4); 4.31 (s, 3 H, NMe); 4.22 (s, 5 H, Cp^{Fc}); 2.44, 1.86 (s, 6 H, C_6H_3*Me*$_2$).

[**2h**]NO_3. ^1H NMR (CD_3OD/D_2O = 1:1): δ/ppm = 5.36, 5.11 (s, 10 H, Cp); 5.21 (s, 1 H, C^2H); 4.67, 4.57 (m, 4 H, C_5H_4); *4.48*, 4.46 (s, 5 H, Cp^{Fc}); *3.98*, 3.97, 3.39 (s, 6 H, NMe).

3. ^{1}H NMR (CD_3OD/D_2O = 3:1): δ/ppm = 4.69. 4.54 (s, 10 H, Cp); 4.23 (s, 5 H, Cp^{Fc}); 2.16, 1.66 (s, 6 H, NMe_2).

4. ^{1}H NMR (CD_3OD/D_2O = 3:1): δ/ppm = 7.46–7.25 (m, 3 H, C_6H_3); 6.87 (s, 1 H, C^2H); 4.45, 4.24, 4.07 (m, 3 H, C_5H_4); 4.08 (s, 5 H, Cp); 3.88 (s, 3 H, NMe); 2.33, 2.22 (s, 6 H, $C_6H_3Me_2$).

Signals in the 5.2-4.5 ppm region are covered by OH resonance.

Figure S42. ^{1}H NMR spectrum (401 MHz, CD_3OD/D_2O = 1:1) of **[2e]CF_3SO_3** after 72 h.

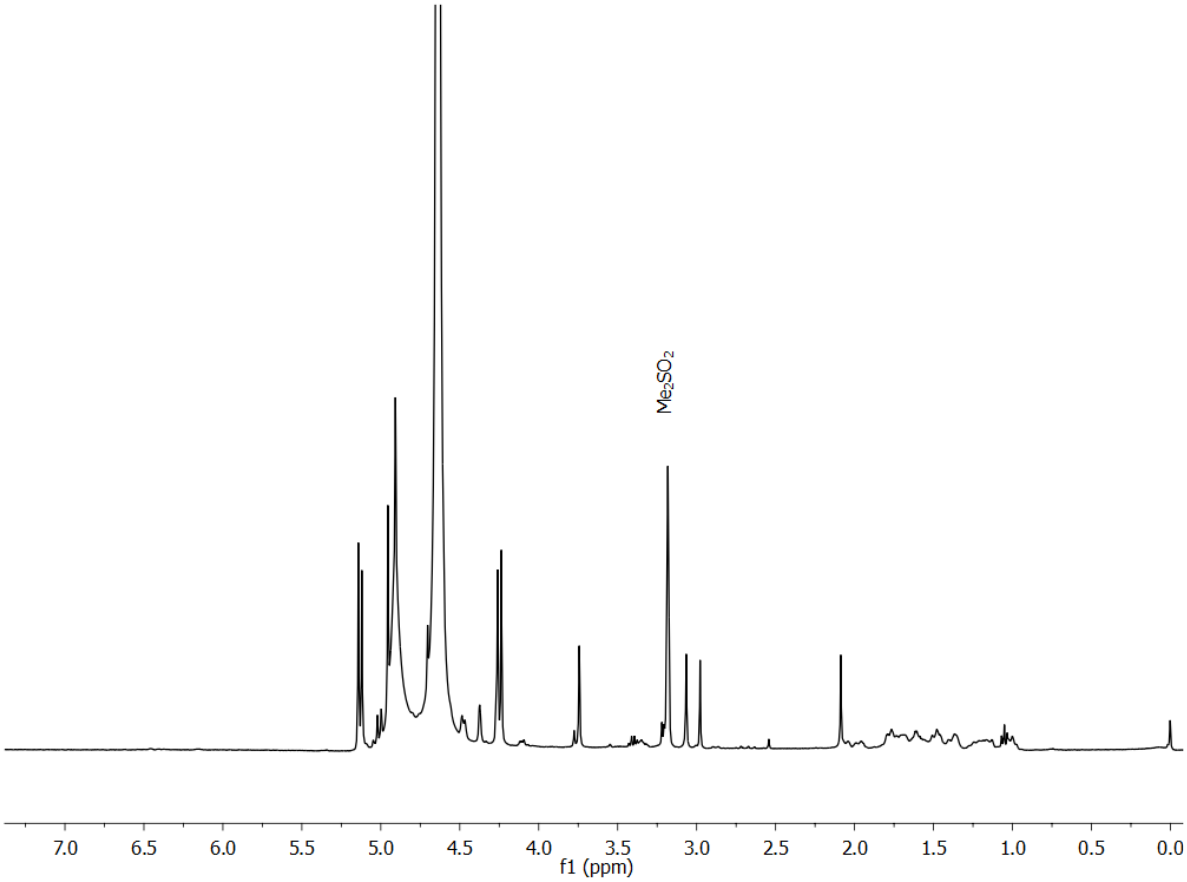

Figure S43. IR spectral changes of a DMSO solution of **[2e]CF_3SO_3** recorded in an OTTLE cell during the progressive increase of the potential from 0.0 to +0.9 V (*vs*. Ag pseudoreference electrode). [N^nBu_4]PF_6 (0.1 mol·dm^{-3}) was used as supporting electrolyte. The absorptions of the solvent and the supporting electrolyte have been subtracted.

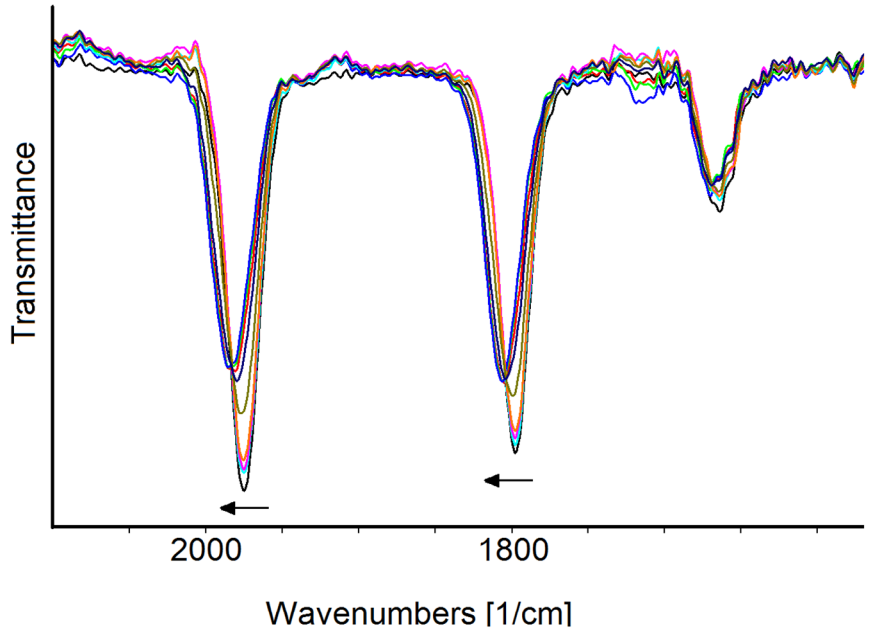

Figure S44. IR spectra of a DMSO solution of **[2e]CF_3SO_3** recorded in an OTTLE cell before (black) and after (red) a slow cyclic voltammetry between 0.0 V and +0.9 V (*vs*. Ag pseudoreference electrode) (scan rate = 1 mV·s^{-1}). [N^nBu_4]PF_6 (0.1 mol dm^{-3}) was used as supporting electrolyte. The absorptions of the solvent and the supporting electrolyte have been subtracted.

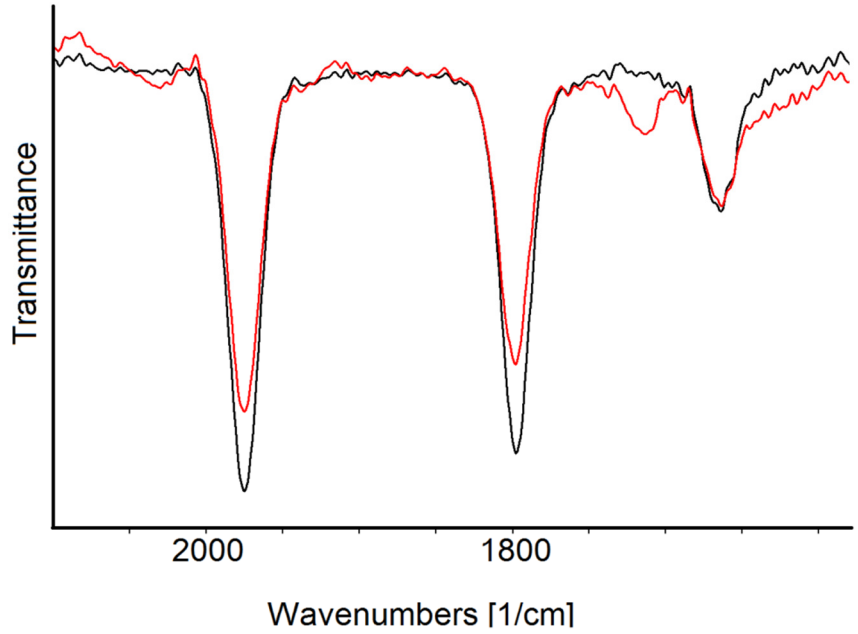

Figure S45. Cyclic voltammetry of **3** recorded at a platinum electrode in 0.1 M $[N^nBu_4]PF_6$/DMSO solution. Scan rate = 0.1 $V \cdot s^{-1}$.

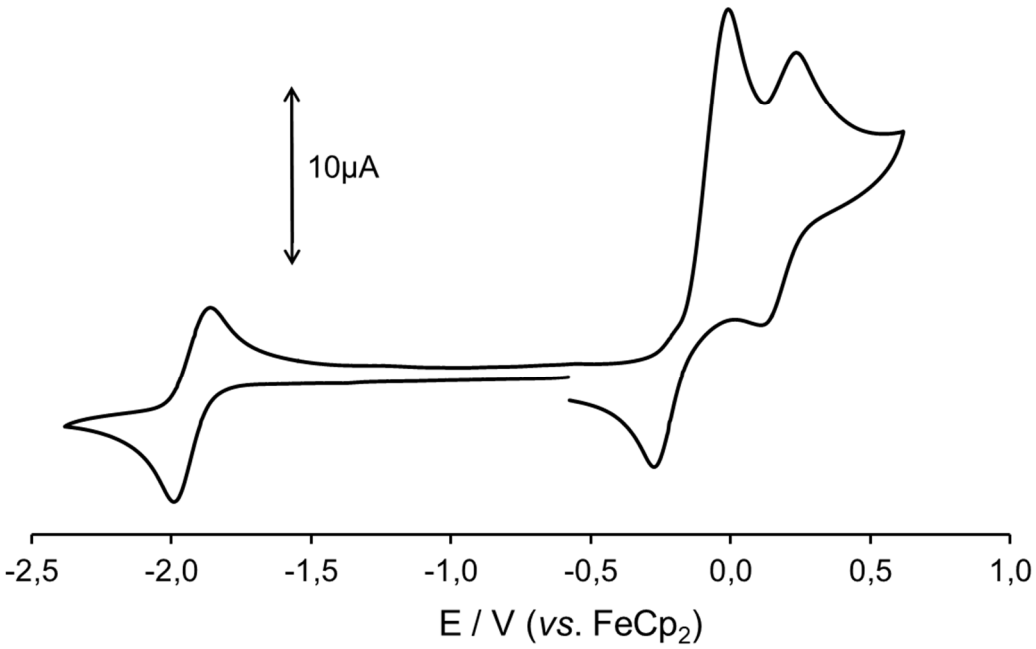

Figure S46. Fluorescence kinetics measurements of intracellular reactive oxygen species (ROS). A2780 cells incubated for 4 hours with 10 μM of complexes and 5% atmosphere of CO_2 at 37 °C. H_2O_2 and menadione (100 μM) were used as positive controls. The black line represents the negative control. Analyses were conducted in triplicate and data are represented as mean ± SD. *Values after 3 hours statistically different from the negative control.

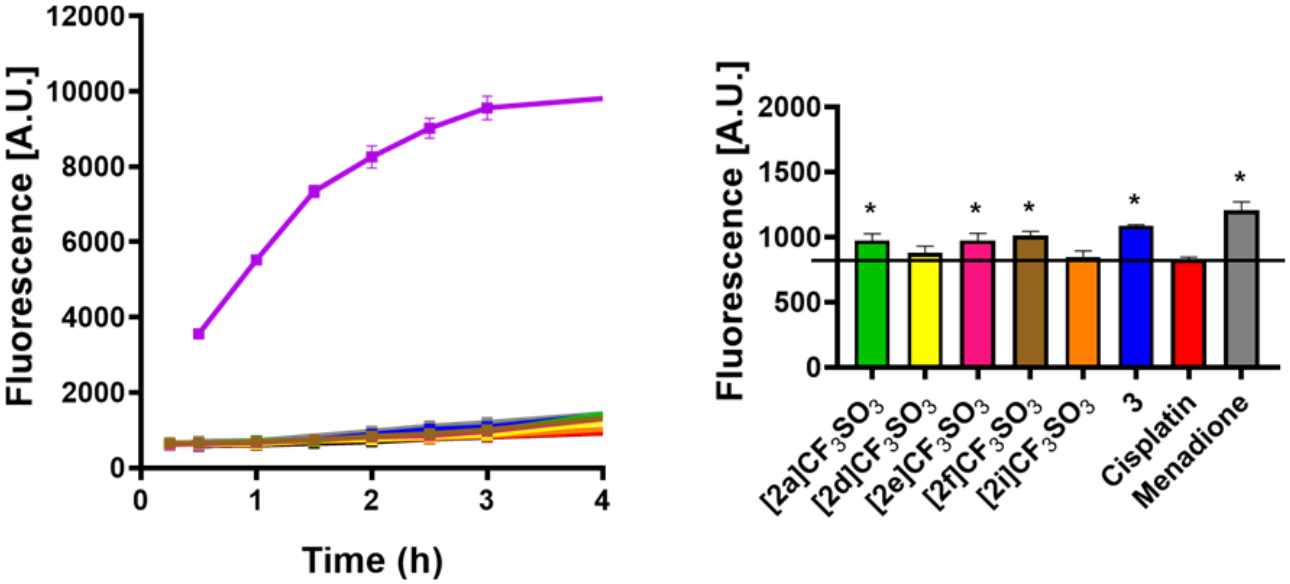

Figure S47. Fluorescence kinetics measurements of intracellular reactive oxygen species (ROS). A2780cisR cells incubated for 4 hours with 10 μM of complexes and 5% atmosphere of CO_2 at 37 °C. H_2O_2 and menadione (100 μM) were used as positive controls. The black line represents the negative control. Analyses were conducted in triplicate and data are represented as mean ± SD. *Values after 3 hours statistically different from the negative control.

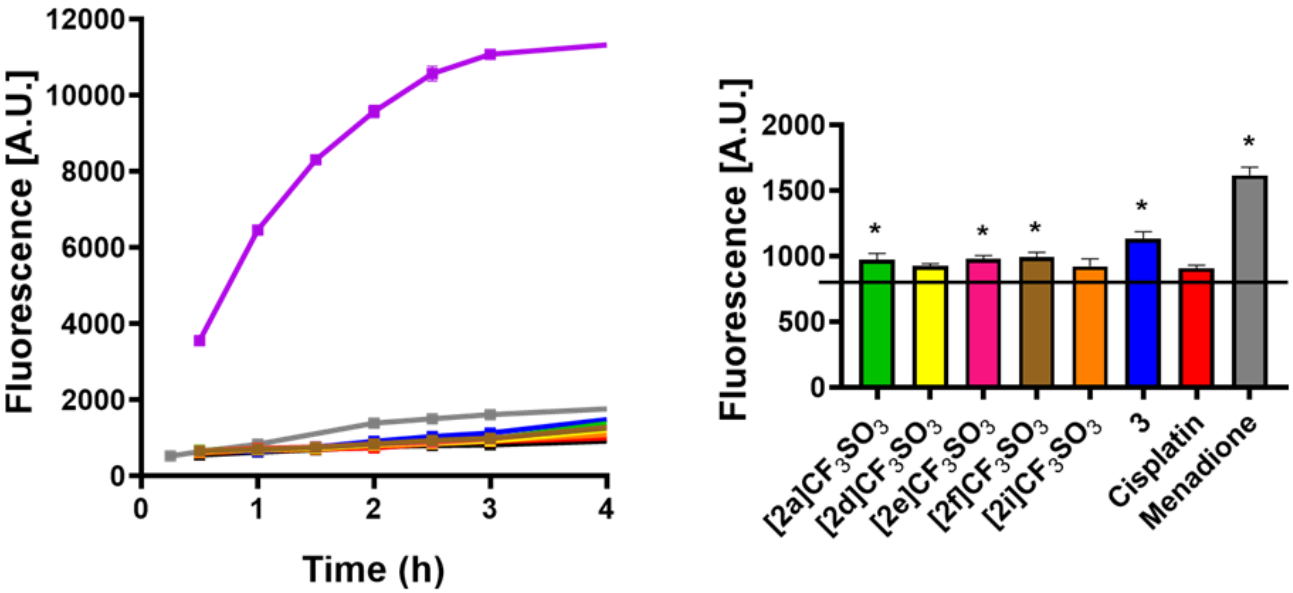

Figure S48. High-resolution ESI mass spectrum of [**2a**]$^+$, 10^{-5} M in 2mM ammonium acetate solution and DMSO 1:1. Experimental isotopic distribution for $C_{33}H_{29}NClFe_3O_2^+$ (black line) *vs* the theoretical one (red lines). Measured *m/z* = 673.99205; theoretical *m/z* = 673.99295; mass error = -1.3 ppm.

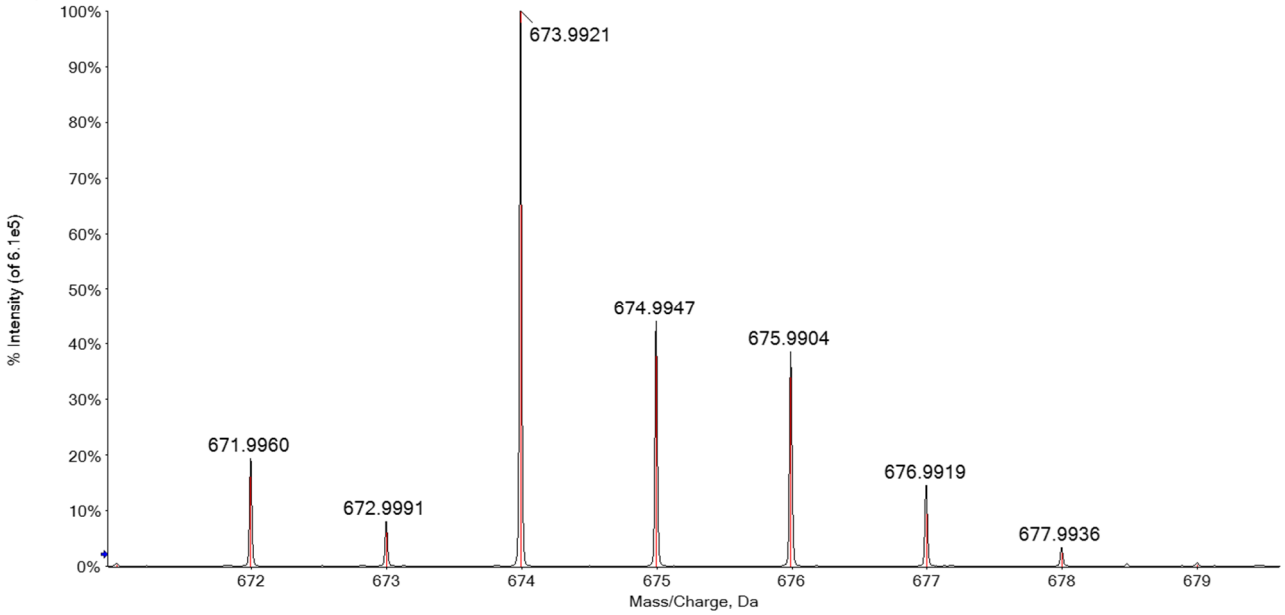

Figure S49. High-resolution ESI mass spectrum of [**2b**]$^+$, 10^{-5} M in 2mM ammonium acetate solution and DMSO 1:1. Experimental isotopic distribution for $C_{33}H_{30}Fe_3NO_3^+$ (black line) *vs* the theoretical one (red lines). Measured *m/z* = 656.02548; theoretical *m/z* = 656.02684; mass error = -2.1 ppm.

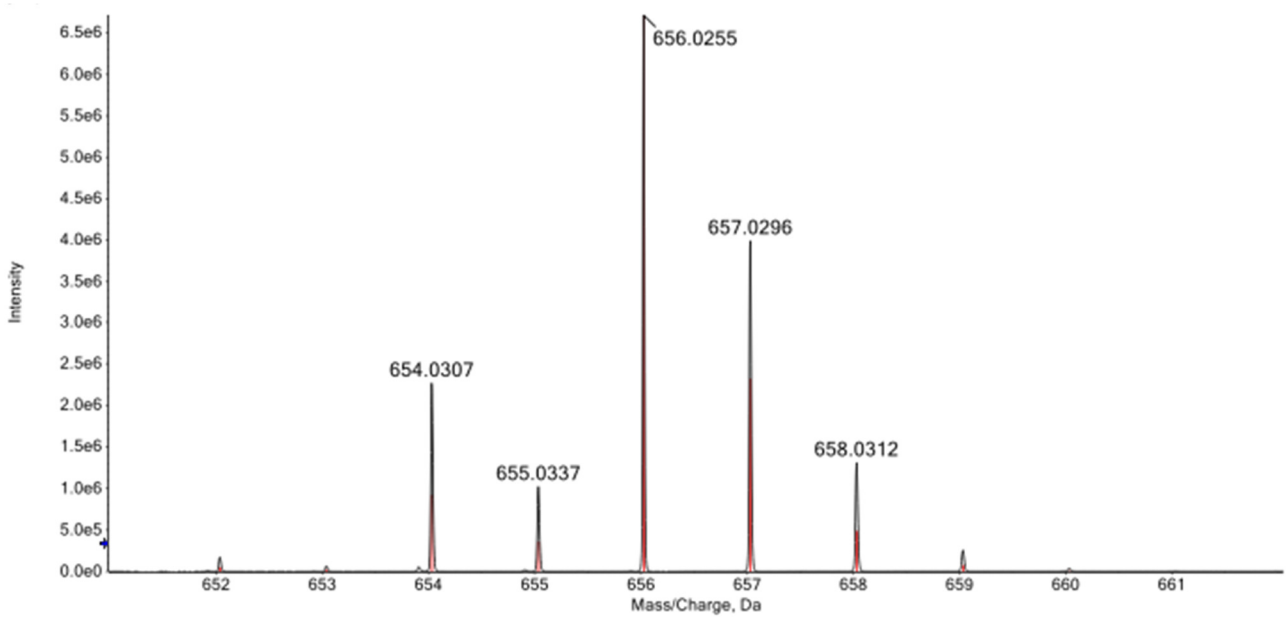

Figure S50. High-resolution ESI mass spectrum of [**2c**]$^+$, 10^{-5} M in 2mM ammonium acetate solution and DMSO 1:1. Experimental isotopic distribution for $C_{36}H_{30}Fe_3NO_2^+$ (black line) *vs* the theoretical one (red lines). Measured *m/z* = 676.03146; theoretical *m/z* = 676.03192; mass error = -0.7 ppm.

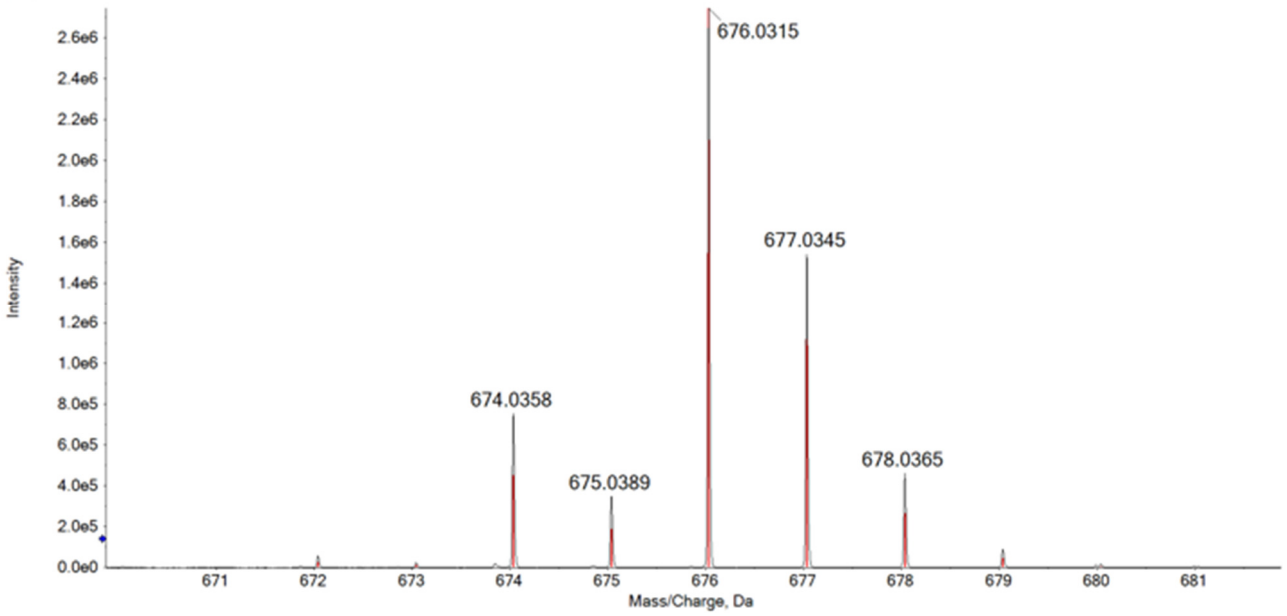

Figure S51. High-resolution ESI mass spectrum of [**2d**]$^+$, 10^{-5} M in 2mM ammonium acetate solution and DMSO 1:1. Experimental isotopic distribution for $C_{33}H_{30}Fe_3NO_2^+$ (black line) *vs* the theoretical one (red lines). Measured *m/z* = 640.03148; theoretical *m/z* = 640.03192; mass error = -0.8 ppm.

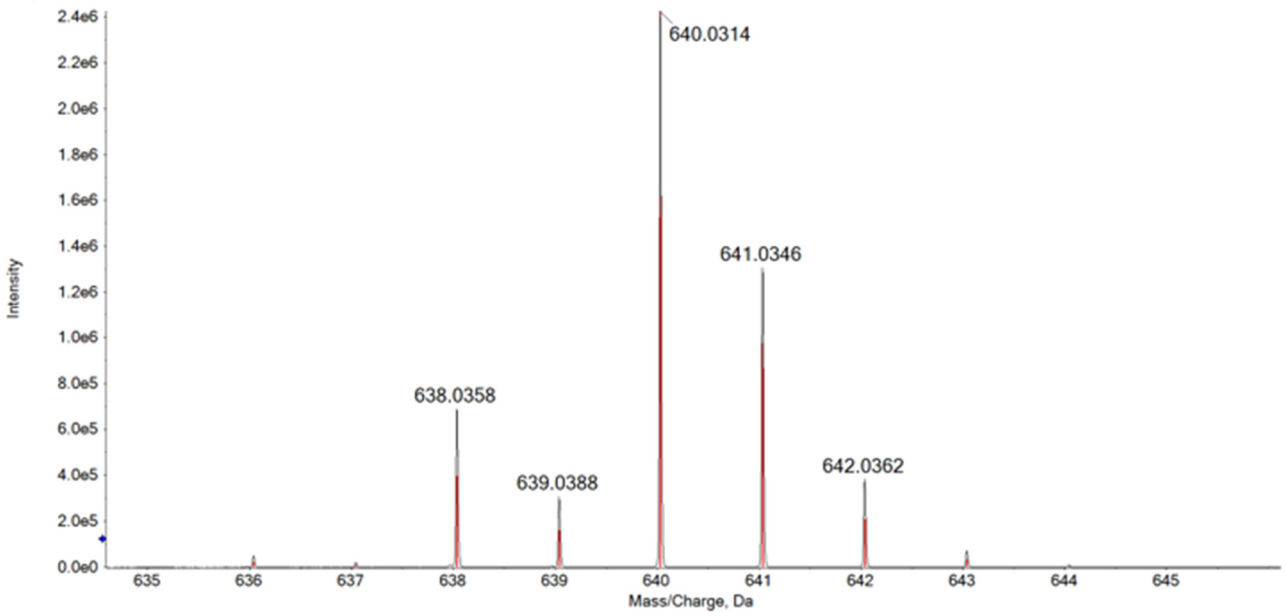

Figure S52. High-resolution ESI mass spectrum of [**2e**]$^+$, 10^{-5} M in 2mM ammonium acetate solution and DMSO 1:1. Experimental isotopic distribution for $C_{32}H_{34}Fe_3NO_2^+$ (black line) *vs* the theoretical one (red lines). Measured *m/z* = 632.06323; theoretical *m/z* = 632.06322; mass error = 0.0 ppm.

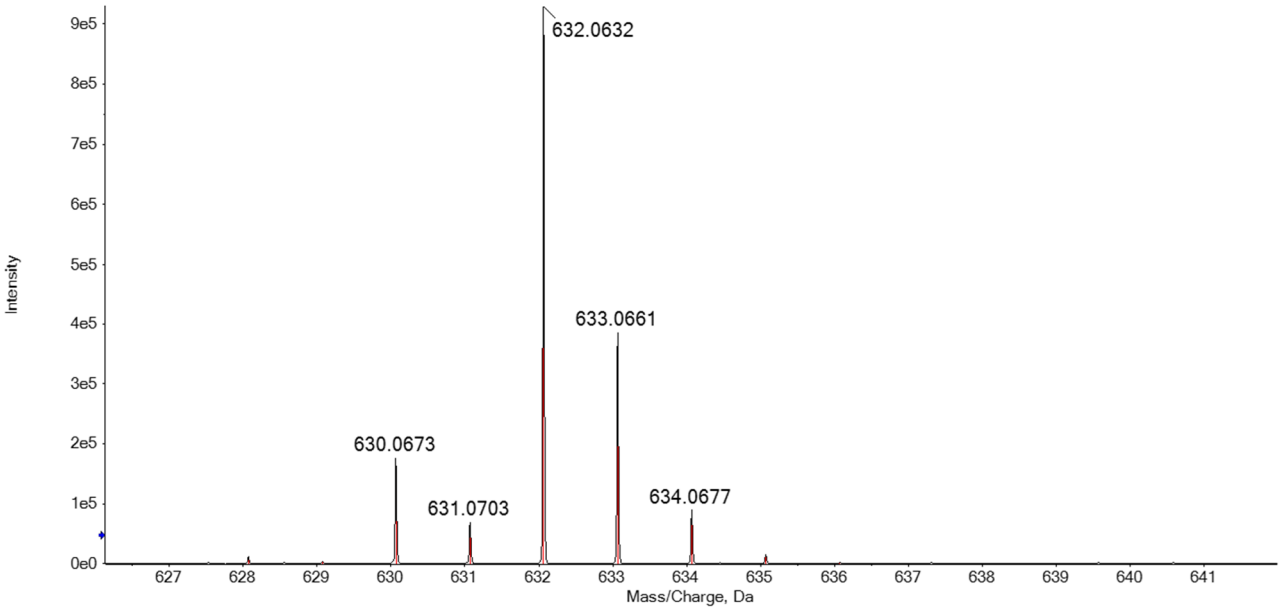

Figure S53. High-resolution ESI mass spectrum of [**2f**]$^+$, 10^{-5} M in 2mM ammonium acetate solution and DMSO 1:1. Experimental isotopic distribution for $C_{29}H_{28}NFe_3O_2^+$ (black line) *vs* the theoretical one (red lines). Measured *m/z* = 590.01680; theoretical *m/z* = 590.01627; mass error = 0.9 ppm.

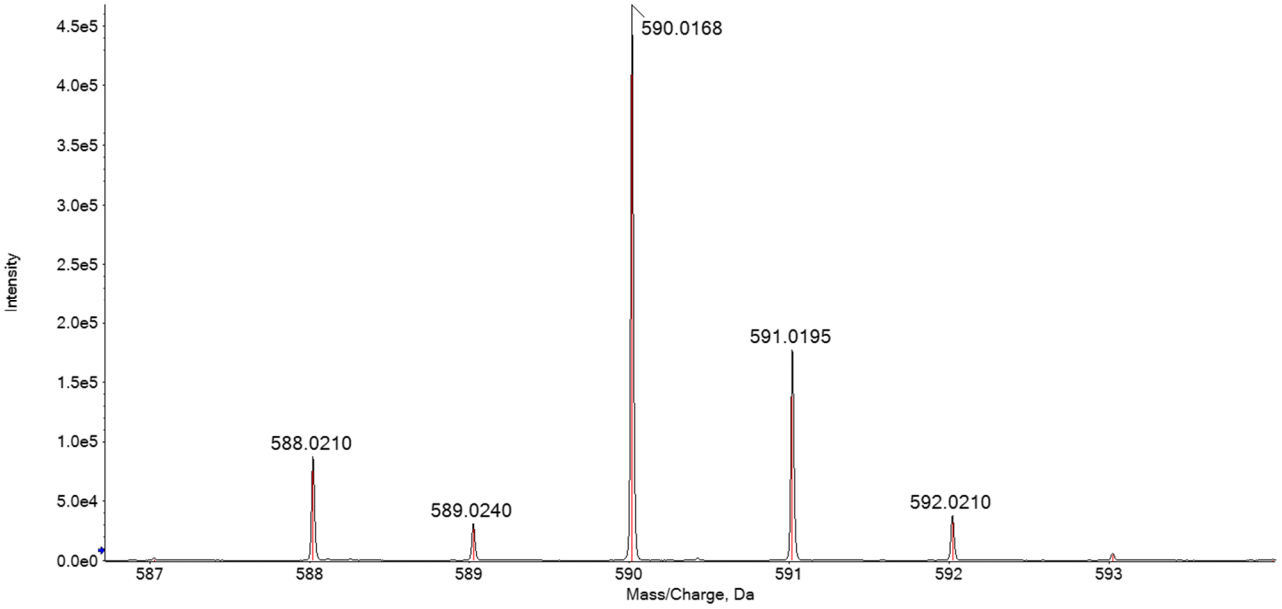

Figure S54. High-resolution ESI mass spectrum of [**2g**]$^+$, 10^{-5} M in 2mM ammonium acetate solution and DMSO 1:1. Experimental isotopic distribution for $C_{39}H_{34}Fe_3NO_2^+$ (black line) *vs* the theoretical one (red lines). Measured *m/z* = 716.06323; theoretical *m/z* = 716.06322; mass error = 0.0 ppm.

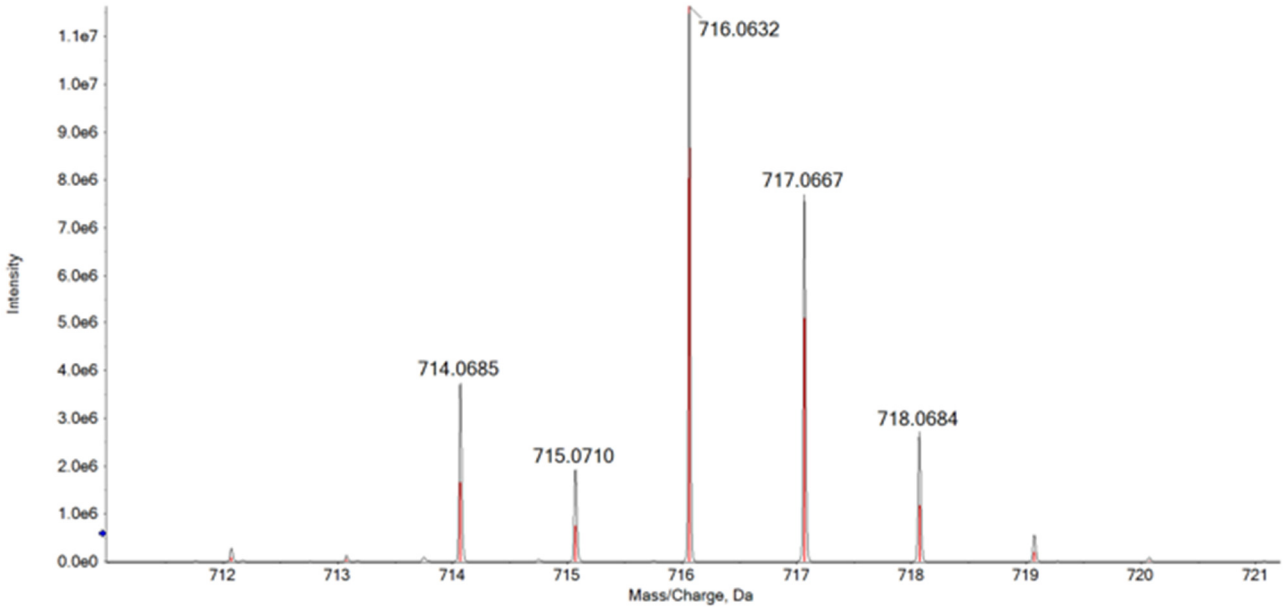

Figure S55. High-resolution ESI mass spectrum of [**2h**]NO_3, 10^{-5} M in 2mM ammonium acetate solution and DMSO 1:1. Experimental isotopic distribution for $C_{27}H_{26}Fe_3NO_2^+$ (black line) *vs* the theoretical one (red lines). Measured *m/z* = 563.99894; theoretical *m/z* = 564.00062; mass error = -3.0 ppm.

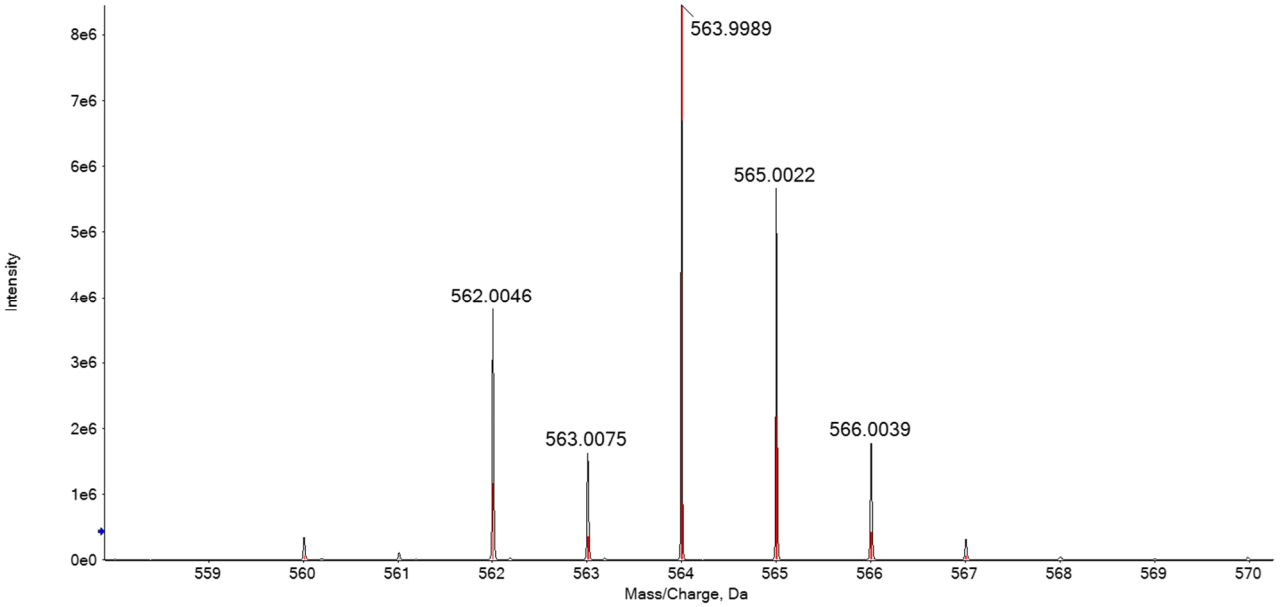

Figure S56. High-resolution ESI mass spectrum of **3**, 10^{-5} M in 2mM ammonium acetate solution and DMSO 1:1. Experimental isotopic distribution for $C_{28}H_{26}Fe_3N_2O_2$ + H^+ (black line) *vs* the theoretical one (red lines). Measured *m/z* = 591.01075; theoretical *m/z* = 591.01152; mass error = -1.3 ppm.

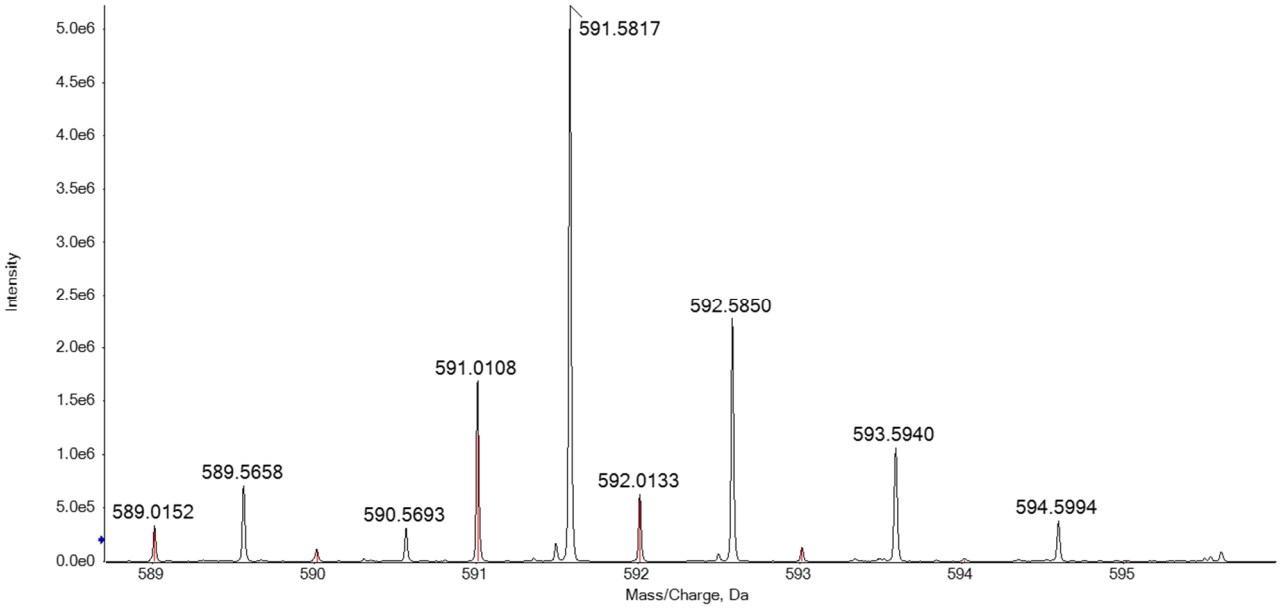

Figure S57. Deconvoluted ESI–MS spectra of Cyt c in 2 mM ammonium acetate solution (pH 6.8), incubated with **[2a]CF_3SO_3** for 24 h at 37 °C. The protein concentration was 10^{-4} M (complex to protein molar ratio = 3).

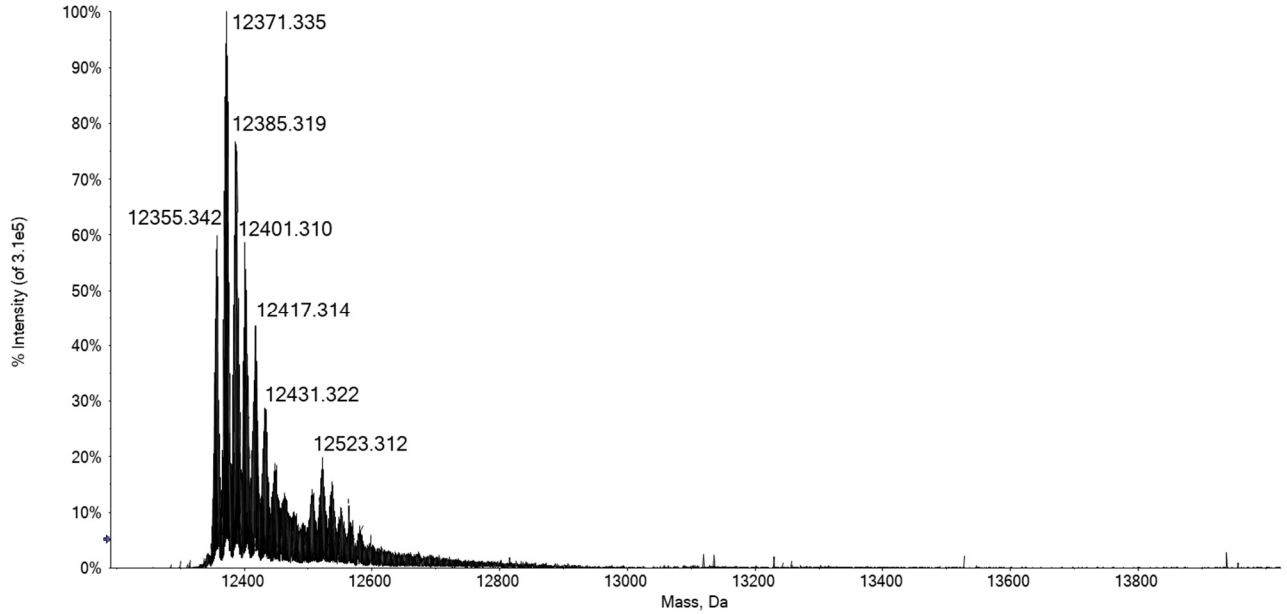

Figure S58. Deconvoluted ESI–MS spectra of HEWL in 2 mM ammonium acetate solution (pH 6.8), incubated with **[2a]CF_3SO_3** for 24 h at 37 °C. The protein concentration was 10^{-4} M (complex to protein molar ratio = 3).

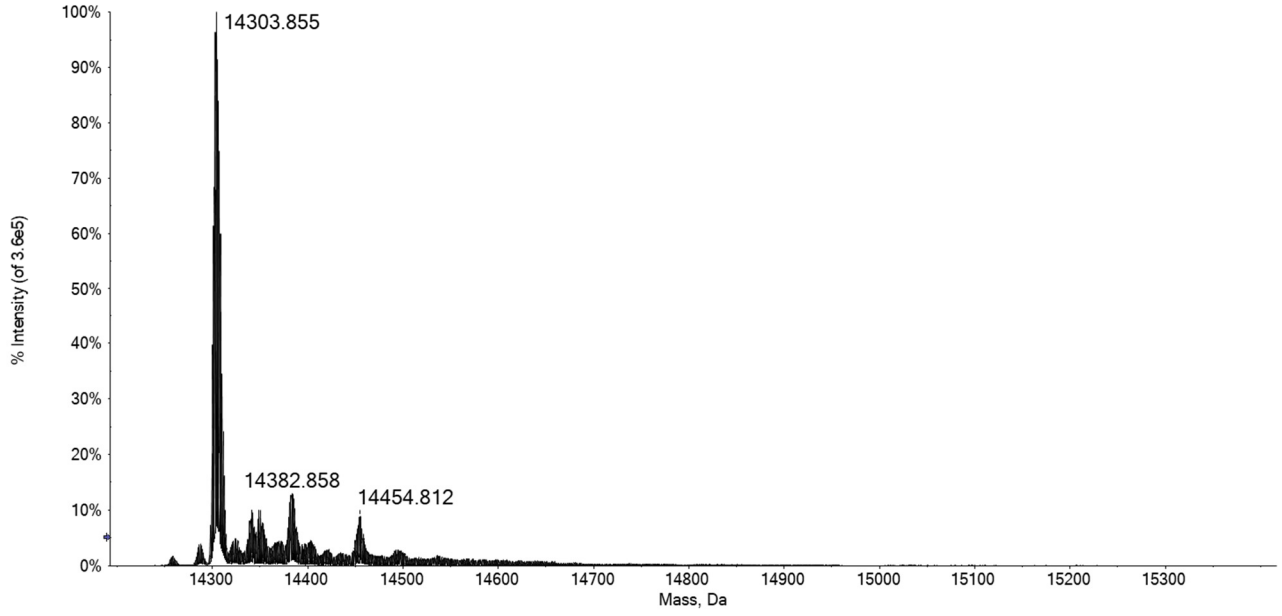

Figure S59. Deconvoluted ESI–MS spectra of Ub in 2 mM ammonium acetate solution (pH 6.8), incubated with **[2a]CF_3SO_3** for 24 h at 37 °C. The protein concentration was 10^{-4} M (complex to protein molar ratio = 3).

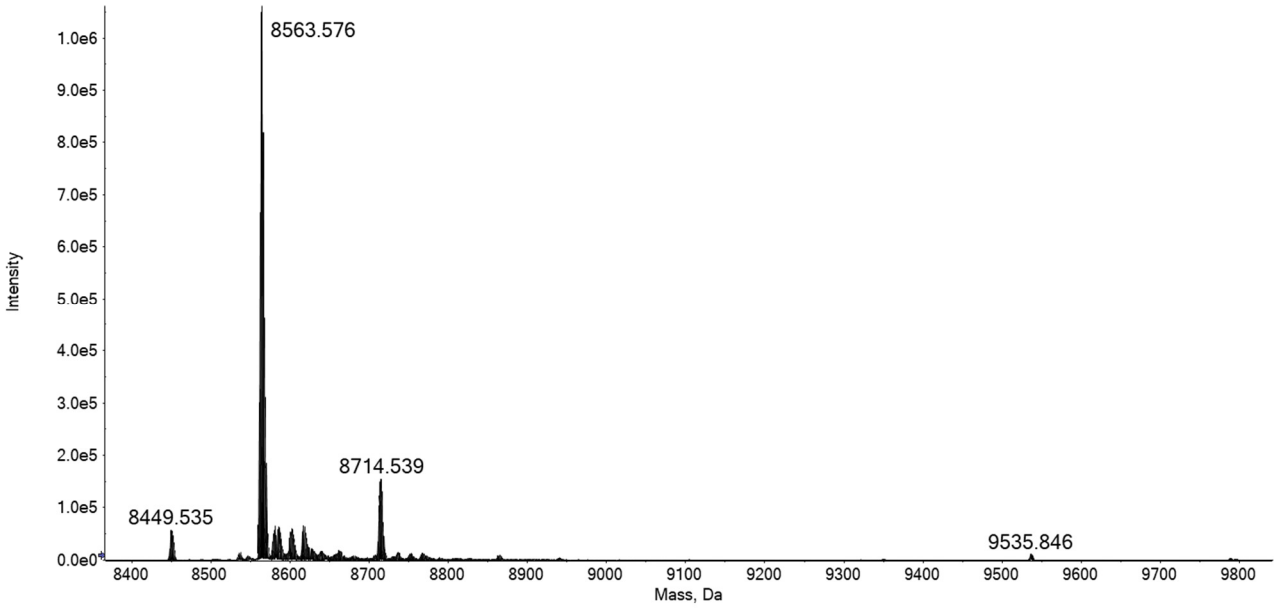

Figure S60. Deconvoluted ESI–MS spectra of BSA in 2 mM ammonium acetate solution (pH 6.8), incubated with **[2a]CF_3SO_3** for 24 h at 37 °C. The protein concentration was 10^{-4} M (complex to protein molar ratio = 3).

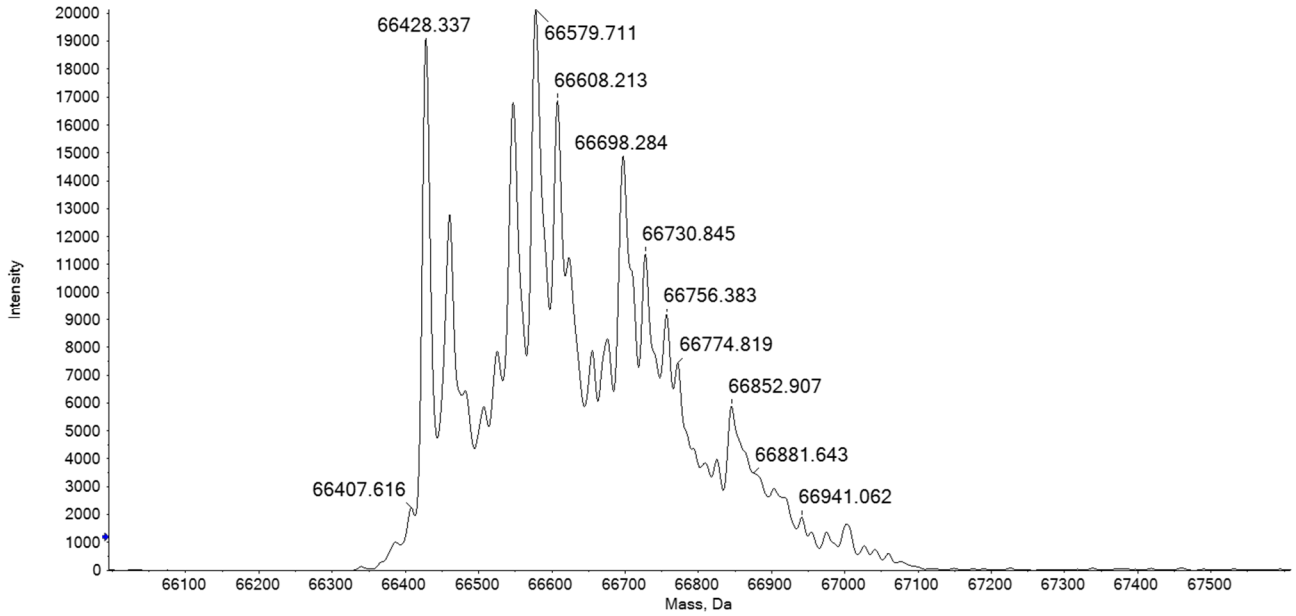

Figure S61. Deconvoluted ESI–MS spectra of SOD in 2 mM ammonium acetate solution (pH 6.8), incubated with **[2a]CF_3SO_3** for 24 h at 37 °C. The protein concentration was 10^{-4} M (complex to protein molar ratio = 3).

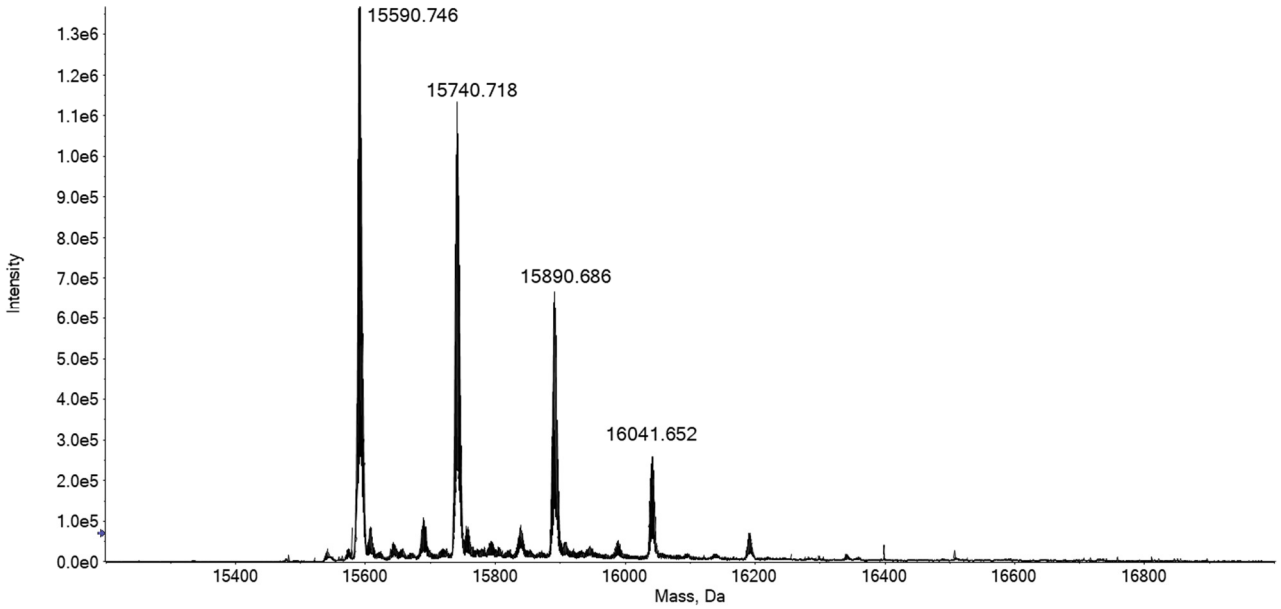

Figure S62. Deconvoluted ESI–MS spectra of hCA I in 2 mM ammonium acetate solution (pH 6.8), incubated with **[2a]CF_3SO_3** for 24 h at 37 °C. The protein concentration was 10^{-4} M (complex to protein molar ratio = 3).

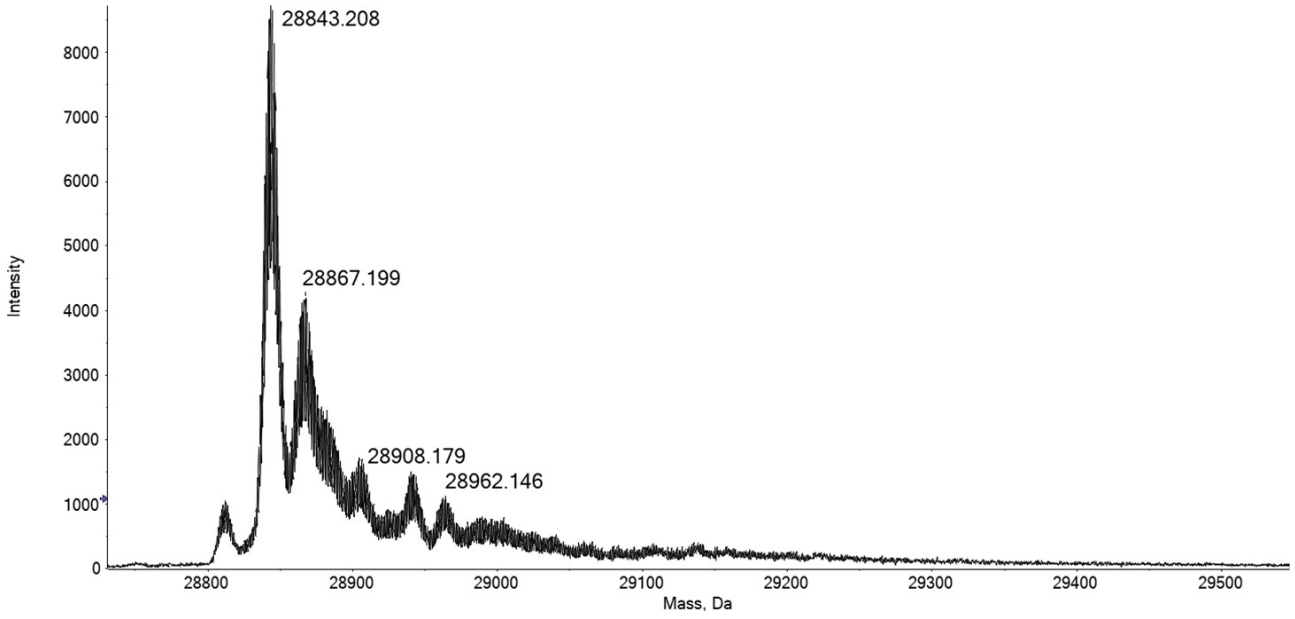

Figure S63. Deconvoluted ESI–MS spectra of ODN2 in water incubated with **[2a]CF_3SO_3** for 24 h at 37 °C. The protein concentration was 10^{-4} M (complex to protein molar ratio = 3).

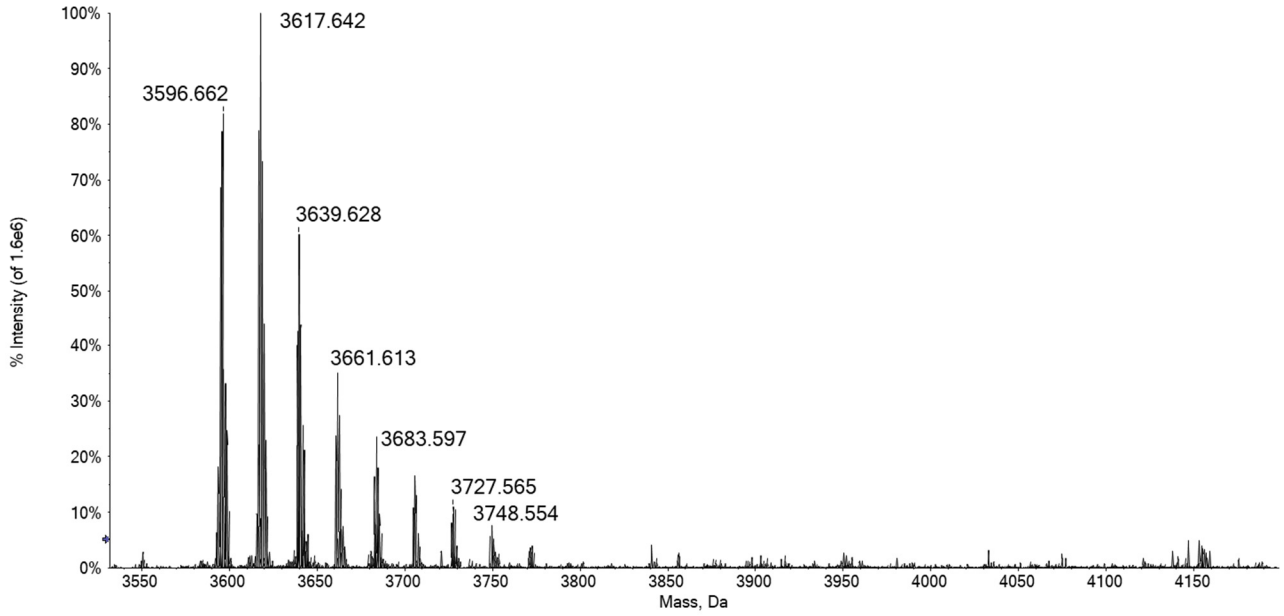

Figure S64. High-resolution ESI mass spectrum of **[2a]CF_3SO_3/TrxR-pept** adduct, $5 \cdot 10^{-6}$ M water. Experimental (black line) *vs* theoretical (red line) isotopic pattern for the [**TrxR-pept** + Fe - H]$^+$ ion ($C_{43}H_{69}N_{14}O_{18}SSeFe$). Measured *m/z* = 1237.31076; theoretical *m/z* = 1237.31441; mass error = -2.9 ppm.

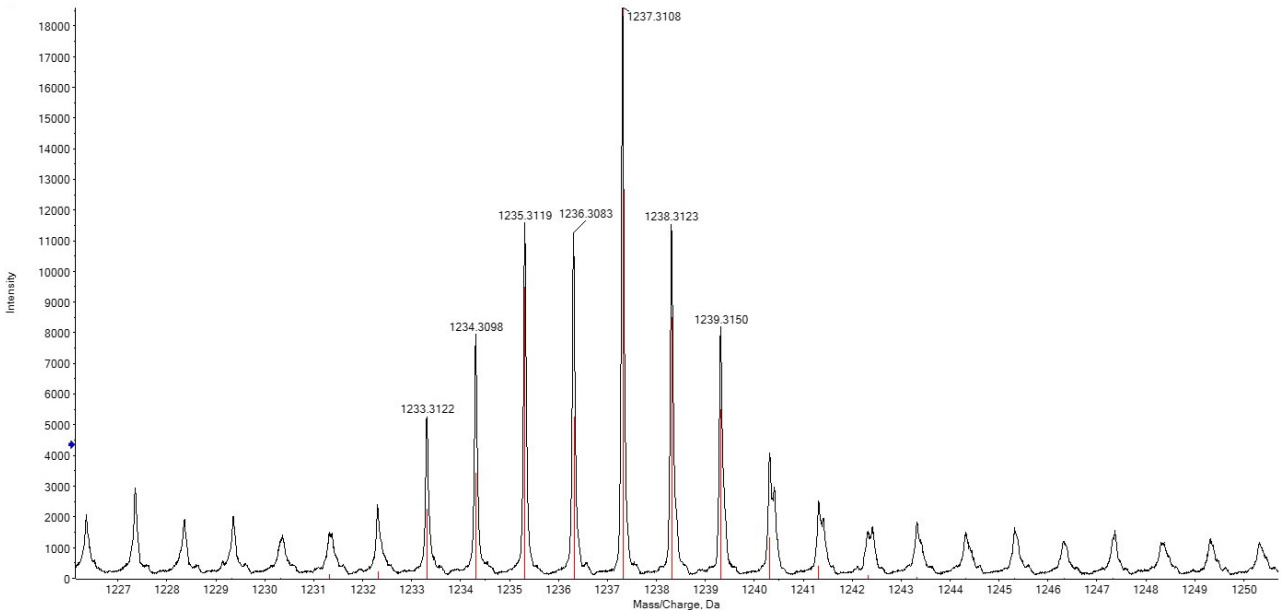

Figure S65. High-resolution ESI mass spectrum of $5 \cdot 10^{-6}$ M solution of **TrxR-pept** in water incubated with **[2f]CF_3SO_3** (1:1 ratio) for 24 h at 37 °C. 0.1% v/v of formic acid was added just before infusion.

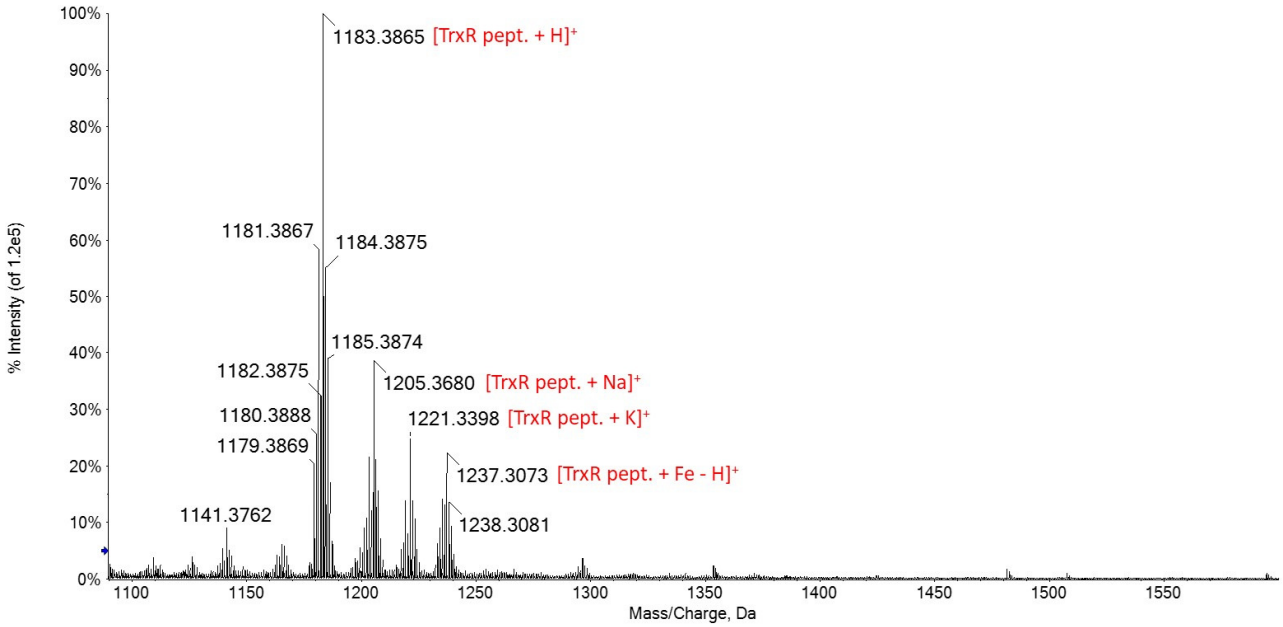

Figure S66. High-resolution ESI mass spectrum of $5 \cdot 10^{-6}$ M solution of **TrxR-pept** in water incubated with **[2h]NO_3** (1:1 ratio) for 24 h at 37 °C. 0.1% v/v of formic acid was added just before infusion.